GLASS AND GLASS-CERAMICS APPLICATION: MATERIALS FOR ENERGY ELECTROLYTES FOR ALL-SOLID-STATE BATTERIES

VIRGINIE VIALLET

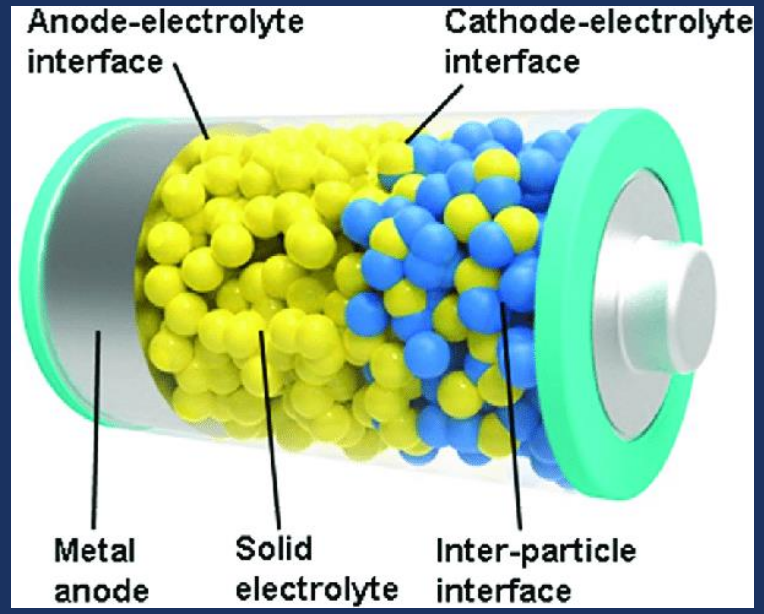

OUTLINE

1 All-Solid-State batteries (ASSB)
Principle, benefits and challenges

2 Glasses and glass-ceramics for ASSB
Requirements and promising solid electrolytes (Li and Na ion conductors)

3 Performances of ASSB
Li-ion, Li-Sulfur and Na-ion batteries

4 Conclusions and perspectives

1

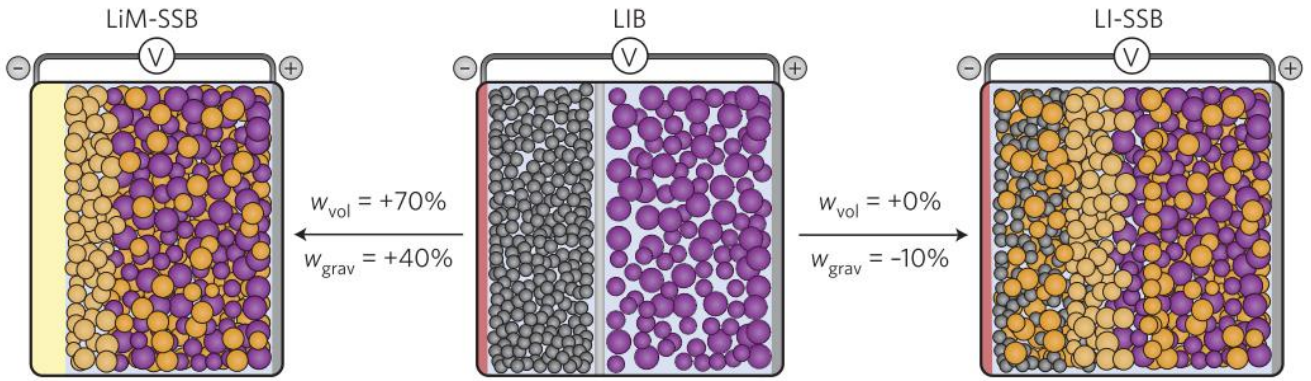

All-Solid-State batteries (ASSB)

Principle, benefits and challenges

Principle of a conventional lithium-ion battery

$C_{graphite}$ $LiCoO_2$

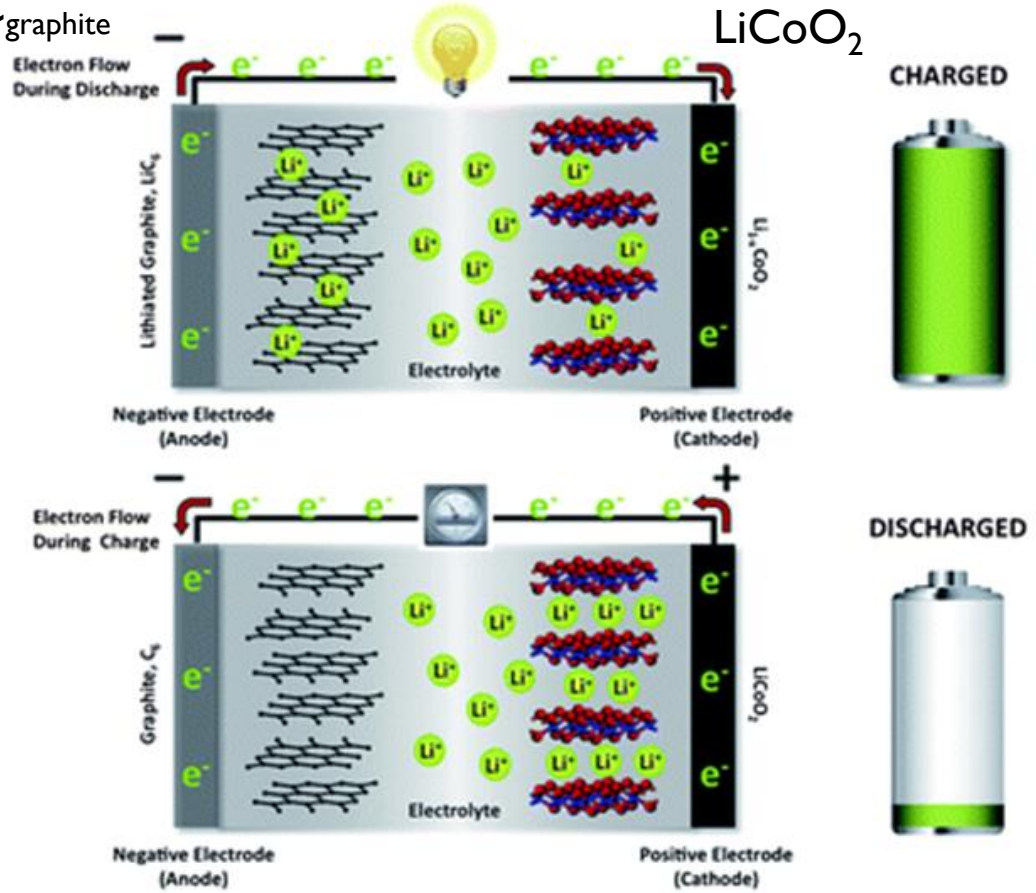

Charge of the battery

$LiCoO_2 \Leftrightarrow Li_{1-x}CoO_2 + x\ Li^+ + x\ e^-$ (x_{max} =0,5)

$6C + x\ Li^+ + x\ e^- \Leftrightarrow Li_xC_6$

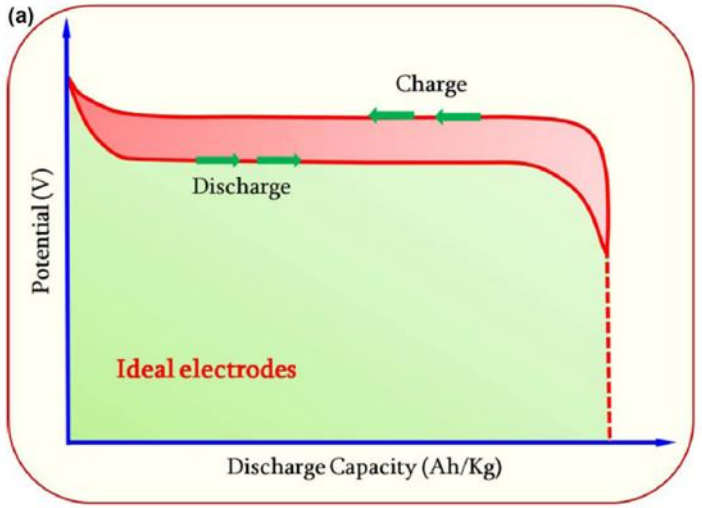

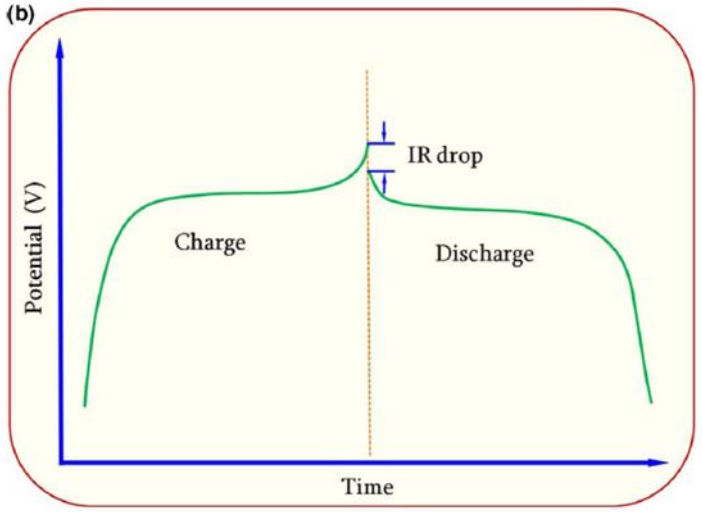

Capacity C (A.h)

$$C = \frac{F.x}{3600.M} = \frac{96485.x}{3600.M}$$

$C_{cathode}(LiCoO_2)_{theo}$ = 135 mAh.g^{-1}

$C_{anode}(C_6)_{theo} = \frac{96485.1}{3600.(6\times12)} =$

= 372 mAh.g^{-1}

Energy

$E = \frac{C_c \times C_a}{C_c + C_a} \times V_{cell}$

Power

$P = V_{cell} \times I$

Current manufactured batteries still face issues:

Flammable organic solvent

- Deformation and ignition due to overheating.
- Leakage of liquid electrolyte.

Dell, Apple batteries Sony
oct. 2006

TESLA Car: LFP/Graphite

USA, oct. 2013

Dreamliner Boeing 787
january 2013,
(Boston, Japon)

Package down-sizing: EV

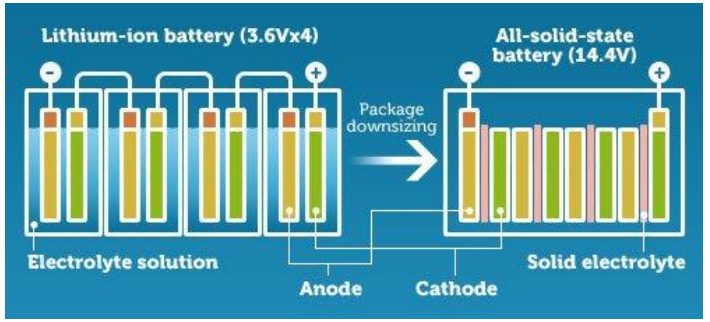

https://www.toyota.com.bh/about/technology/environmental-technology/next-generation-secondary-batteries/

Energy density increase

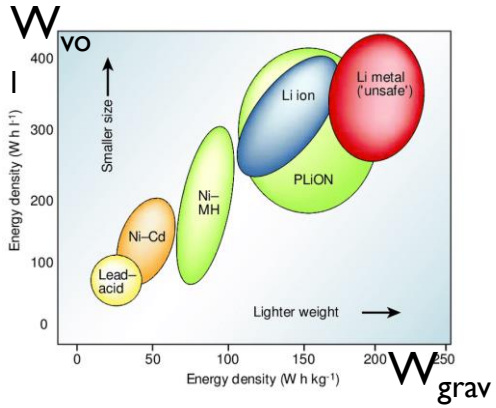

Energy density
= capacity x potential

volumetric and gravimetric energy densities (W_{vol}, W_{grav})

positive electrode materials

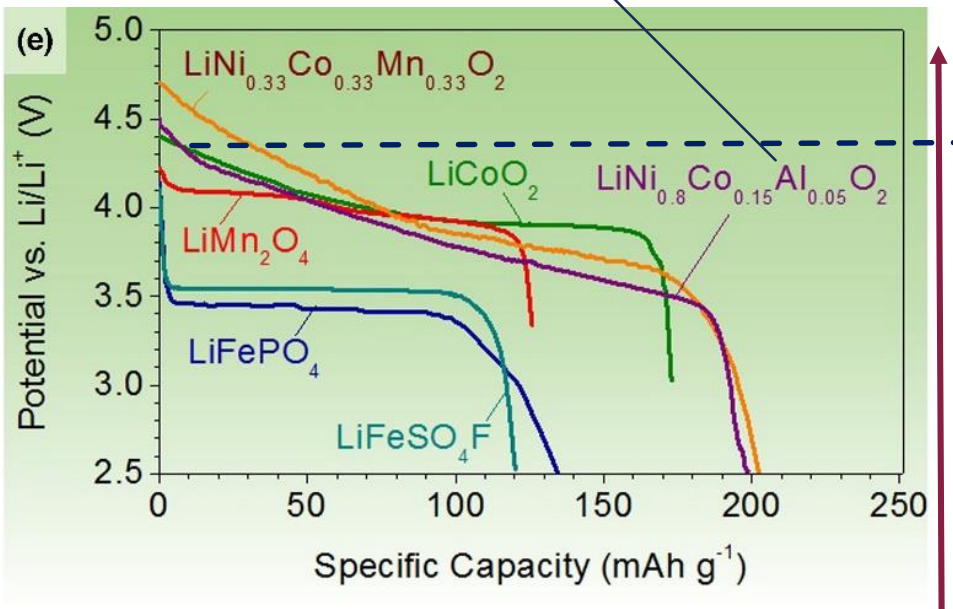

high-energy cathode material

$LiCoPO_4$	4.8 V *vs.* Li/Li^+	~801 Wh kg^{-1}
$LiNi_{0.5}Mn_{1.5}O_4$	4.7 V *vs.* Li/Li^+	~690 Wh kg^{-1}

Stability window
Solid electrolyte?

Stability window
liquid electrolyte

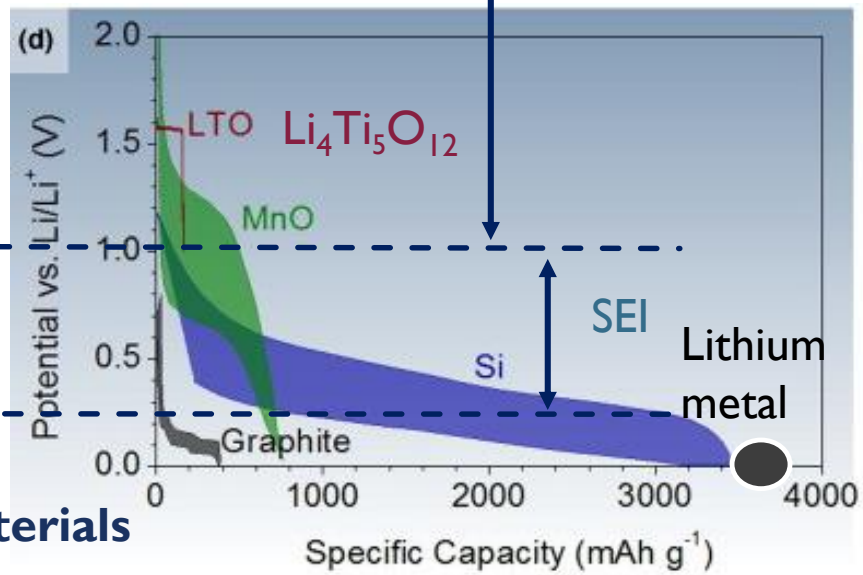

lithium (Li) metal

- high theoretical specific capacity (3860 mAh g^{-1}),
- low density (0.59 g cm^{-3})
- and the lowest negative electrochemical potential

⇒ ideal negative electrode for the high energy density rechargeable batteries

negative electrode materials

Energy density increase

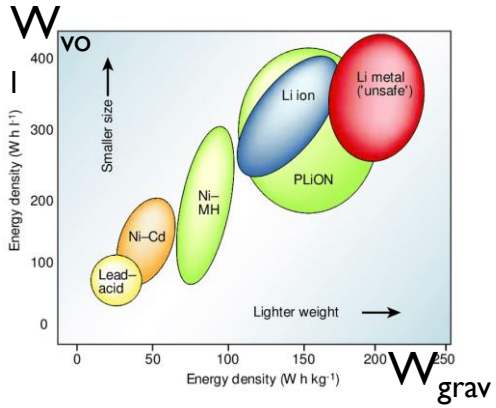

Energy density
= capacity x potential

volumetric and gravimetric energy densities (W_{vol}, W_{grav})

Typical battery architectures for the conventional lithium-ion and all-solid-state batteries (ASSB)

Solid state battery with a lithium-metal anode

Conventional lithium-ion batteries

Lithium ion all-solid-state battery with a conventional anode

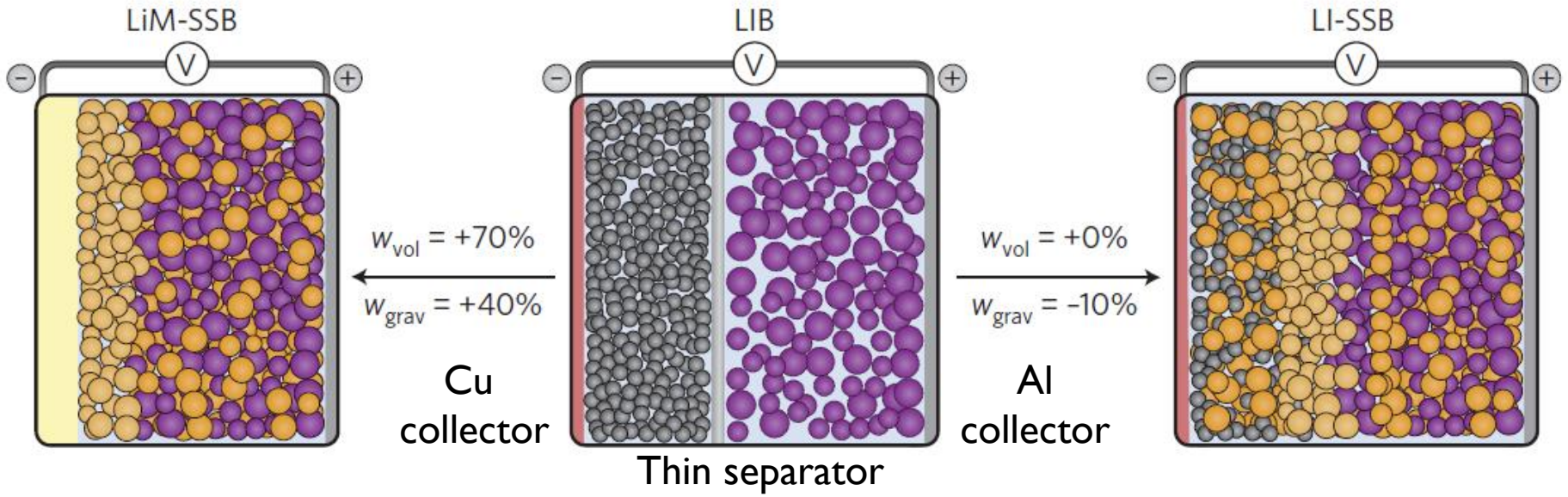

$$Q(Li_{metal})_{theo} = \frac{96485 \times 1}{3600 \times (6.94)} = 3862 \text{ mAh.g}^{-1}$$

Porous anode
Negative electrode
Graphite
372 mAh.g^{-1}

Porous cathode
Positive electrode
$LiCoO_2$
135 mAh.g^{-1}

J. Janek & W. G. Zeier, Nature Energy, Vol. 1 , 2016

Interface

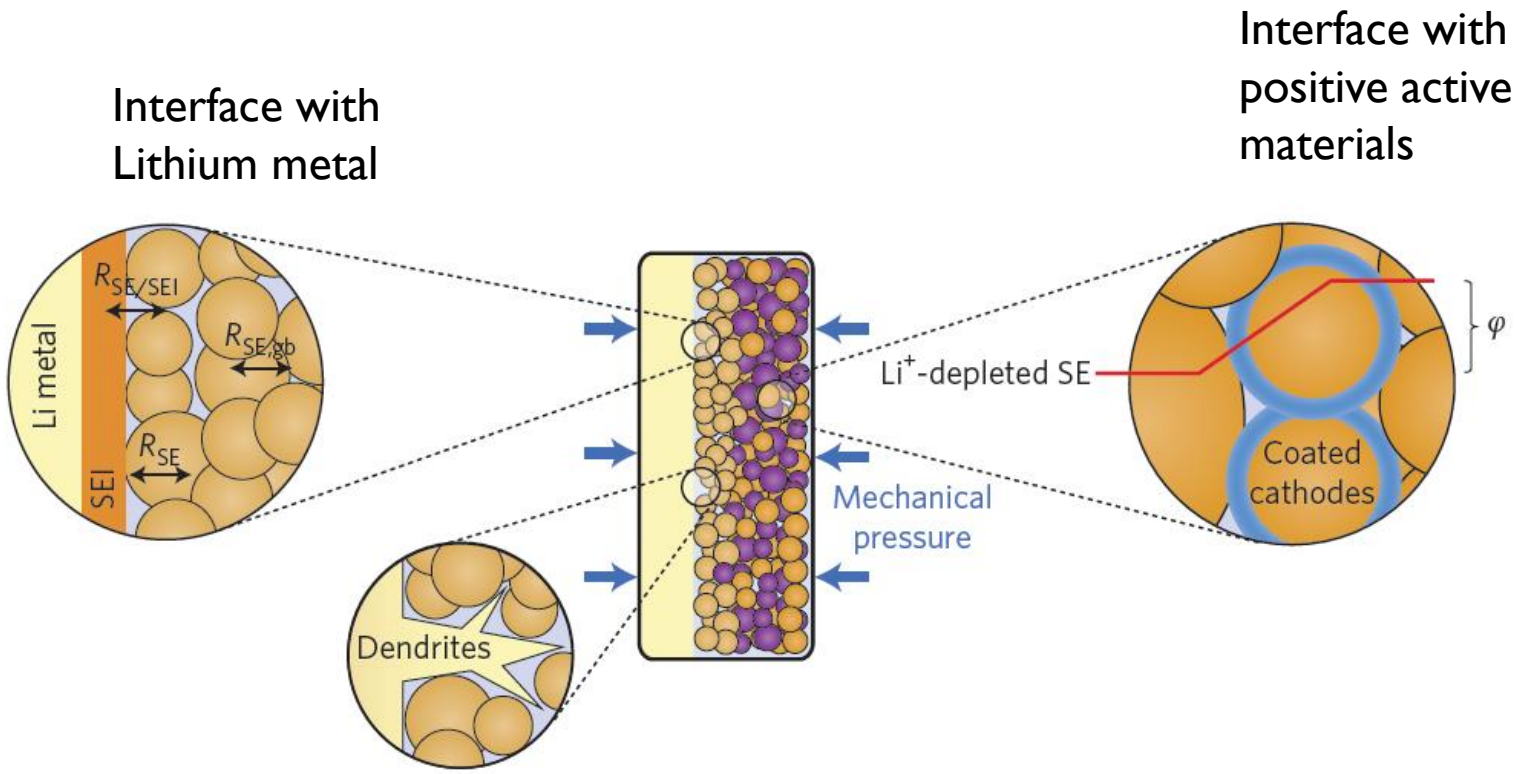

electric resistance between electrolytes and electrode materials is large because of the limited contact area
⇒ solid composite electrodes ensuring sufficient electronic and ionic percolation have to be formed

J. Janek & W. G. Zeier, Nature Energy, Vol. 1 , 2016

Solid electrolyte

Ranking of properties of solid electrolytes (5 = best, 1 = worst).

Low $\sigma_{electron} < 10^{-12}$ S.cm^{-1}

$\sigma_{ion} > 10^{-4}$ S.cm^{-1}

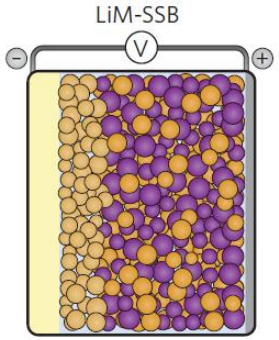

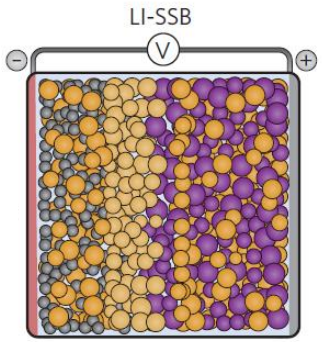

L. Han *et al*, Frontiers in energy research, Vol. 8, article 202, 2020

2

Glasses and glass-ceramics for ASSB

Requirements and promising solid electrolytes

Which ionic conductors?

Li^+
Na^+
Ag^+ (not developed in this presention as less results)

Inorganic solids
(crystalline, glass or glass-ceramics)

Organic Solid Polymers

Solid Polymer Electrolytes (SPE)
Gel Polymer Electrolytes (GPE)
80 °C to operate (BlueCar)
(not developed in this presention)

1,530 Publications (glass & glass-ceramic)
Total From 1900 to 2021

Ball-milling

Solvent assisted technique

Classical melt quenching or twin-roller

Na

Ag

Li

1970 1980 1990 2000 2010 2014 2020

Na_2S-GeS_2
Na_2S-SiS_2
Na_2S-P_2S_5

Na_3PS_4-Na_4SiS_4

AgI-Ag_2SeO_4

Li_2O-SiO_2-Al_2O_3

Anion doped

Li_2S-P_2S_5
Li_2S-P_2S_5-LiI
Li_2S-B_2S_3-LiI
Li_2S-$(Ge,Si)S_2$-LiI

1993
LIPON*

1997
LAGP $Li_{1.5}Al_{0.5}Ge_{1.5}(PO_4)_3$
LATP $Li_{1.3}Al_{0.3}Ti_{1.7}(PO_4)_3$

Li_2S-P_2S_5-SiS_2
Li_2S-P_2S_5-LiX (Br, Cl, I)
Li_2S-P_2S_5 -B_2S_3
Li_2S-P_2S_5
Li_2S- SiS_2
Li_2S- SiS_2 – Li_3PO_4
Li_2S- SiS_2 – Li_2SO_4
Li_2S- SiS_2 – Li_4SiO_4
Li_2S- SiS_2 – Li_4GeO_4

Li_2S-P_2S_5 75-25 or 80-20
⇒ Glass ceramic $Li_7P_3S_{11}$
Glass ceramic Li_3PS_4-Li_4SiS_4

Li_2S-P_2S_5 - Li_2O
Li_2S- SiS_2 - Li_4SiO_4

2012
Argyrodite
Li_6PS_5X (X=Cl, Br, I)
Glass-ceramic

2012
Antiperovskite
Li_3ClO

$Li_7P_{2.9}Sb_{0.1}S_{10.75}O_{0.25}$

* microbatteries

Glass formation

1970 1980 1990 1997 2000 2010 2020

Classical routes
From the 1970s to 2000

New synthetic routes
Since the 2000s

Melting
+ quenching

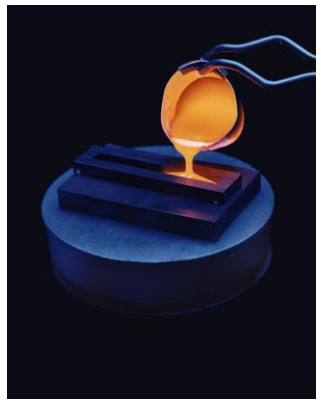

thermal-image furnace
and twin roller

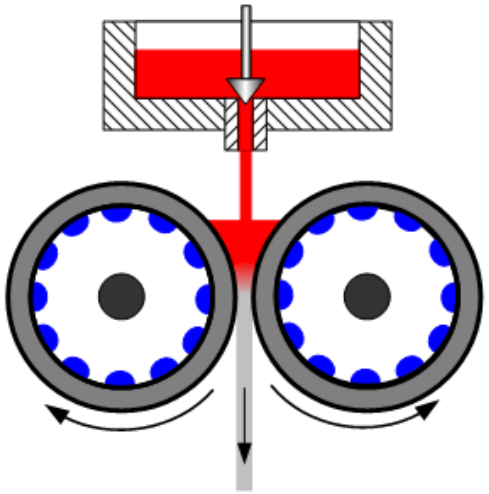

Ball-milling (BM)

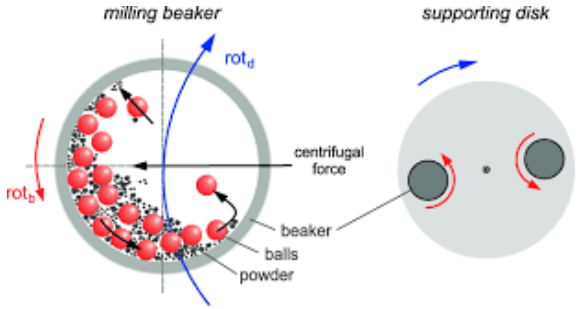

Nature of the balls and jarrs
Speed
Duration of milling
…

Solvent assisted synthesis

Which ionic conductors?

Li^+
Na^+
Ag^+ (not developed as less results)

Inorganic solids
(crystalline, glass or glass-ceramics)

Oxides and phosphates

- Handling under room atmosphere

- Brittle
and often experience mechanical failure through cracking
- Sintering at high temperature

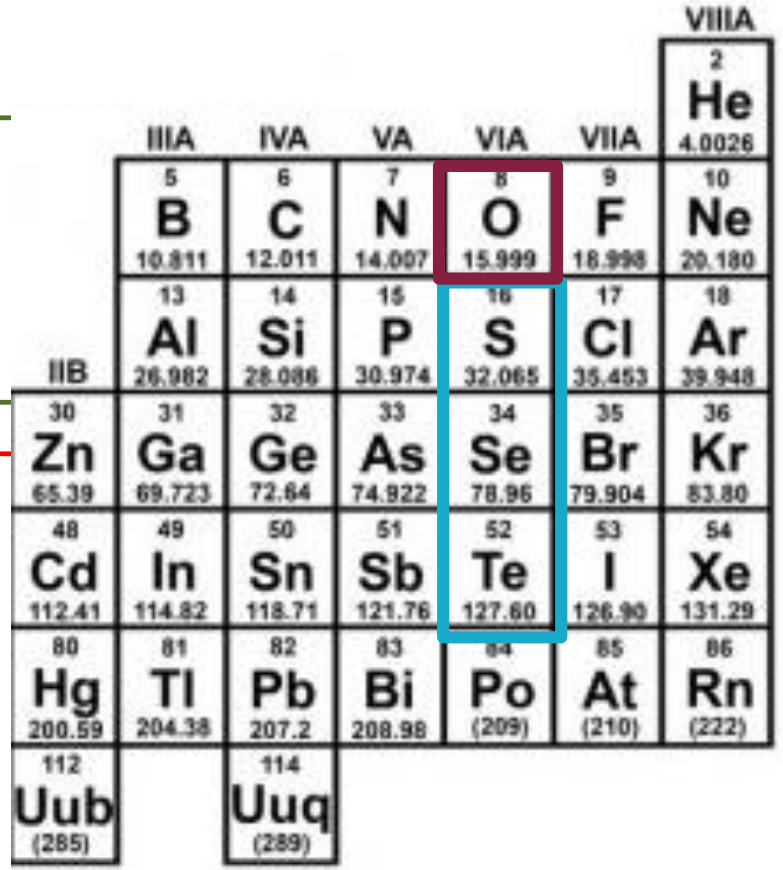

Chalcogenides

Sulfides are ductile
easily form dense cathode and anode composites

- But moisture sensitive:
partial hydrolysis &H_2S toxic gas formation
⇒ Drop ionic conductivity
⇒ Safety problems

interest of glasses compared to crystallized phases

- Wide selection of composition
  $(100-x)Li_2S$-xP_2S_5
  Li_2S-P_2S_5- LiI
  Li_2S-SiS_2
- Non flammability
- Easy film formation
- Ionic conductivity generally > Ionic conductivity crystal
- Single cation conduction
  Li^+ for Li conducting glasses
  Na^+ for Na conducting glasses

Heating

- Stable crystalline phase with lower Grain-Boundary resistance
  LATP
  LAGP
- Glass-ceramics
  80-20 Li_2S-P_2S_5
  70-30 Li_2S-P_2S_5
  $Li_7P_3S_{11}$
  Argyrodite Li_6PS_5X (X = Cl, Br, I)
- Superionic conductive crystal
  $Li_7P_3S_{11}$
  Na_3PS_4

Glass-ceramic formation

Schematic description of the conversion of a glass into a glass-ceramic.

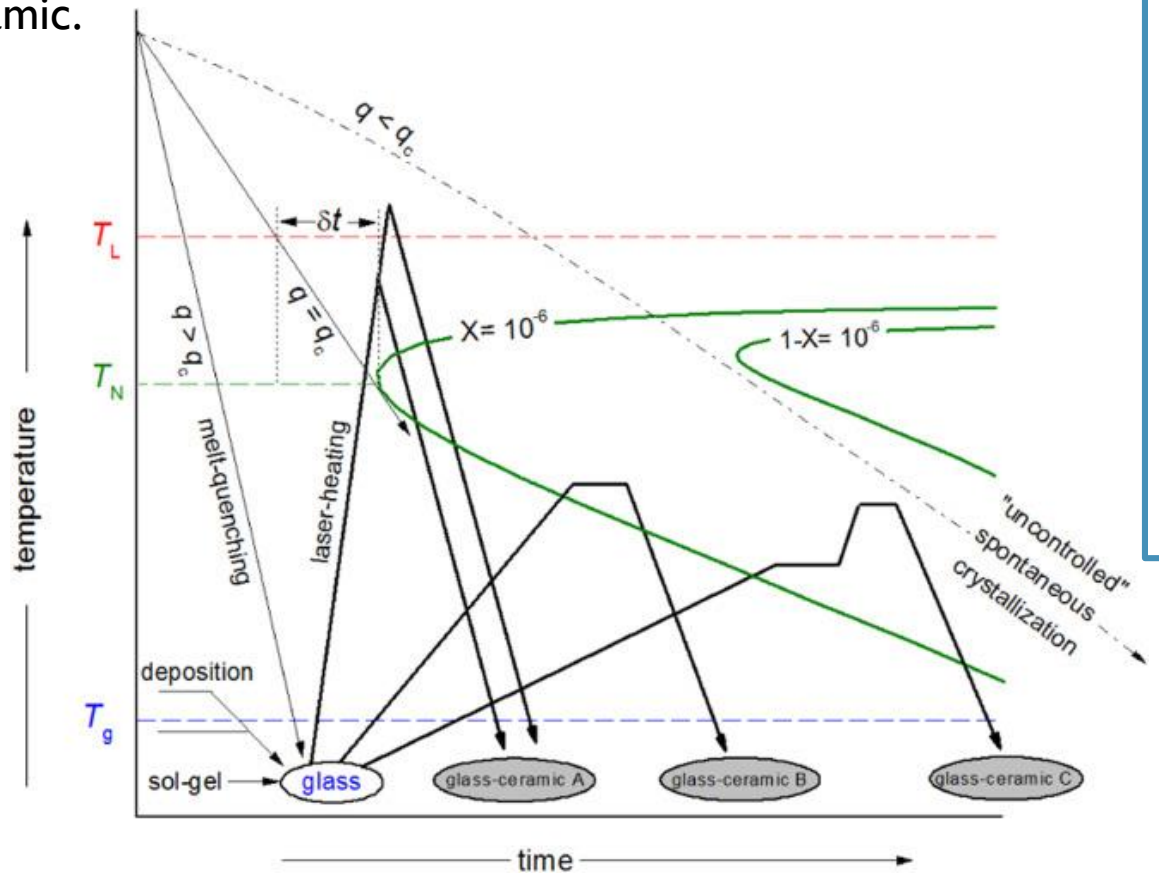

J. Deubener *et al.*, Journal of Non-Crystalline Solids Volume 501, 2018, Pages 3-10
Updated definition of glass-ceramics

The critical cooling rate is $q_c = (T_L - T_N) / \delta t$
with T_L = liquidus temperature,
and T_N = "nose temperature"
(=temperature at which the time δt to achieve a crystal fraction of 10^{-6} is shortest).

Glass formation by melt-quenching for $q \geq qc$.
"Uncontrolled" spontaneous crystallization for $q < qc$.

- ✓ glass-ceramic A obtained during cooling,
- ✓ glass-ceramics B and C converted by single and double-stage heat-treatments, respectively.

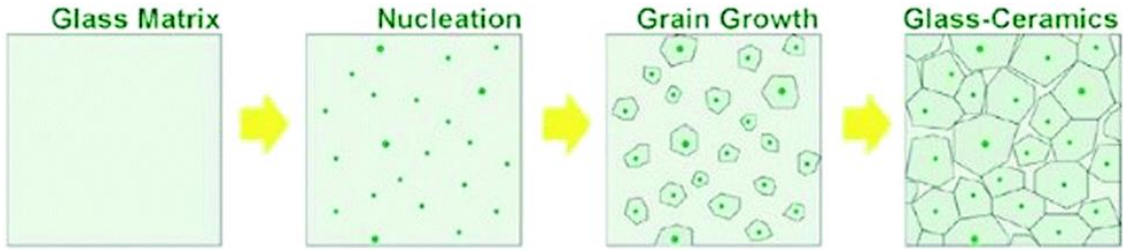

S. Liu et al, J. Mater. Chem. C, 2019, 7, 15118-15135

Superionic conductive crystal

Volume changes from glass to crystal with increasing temperature

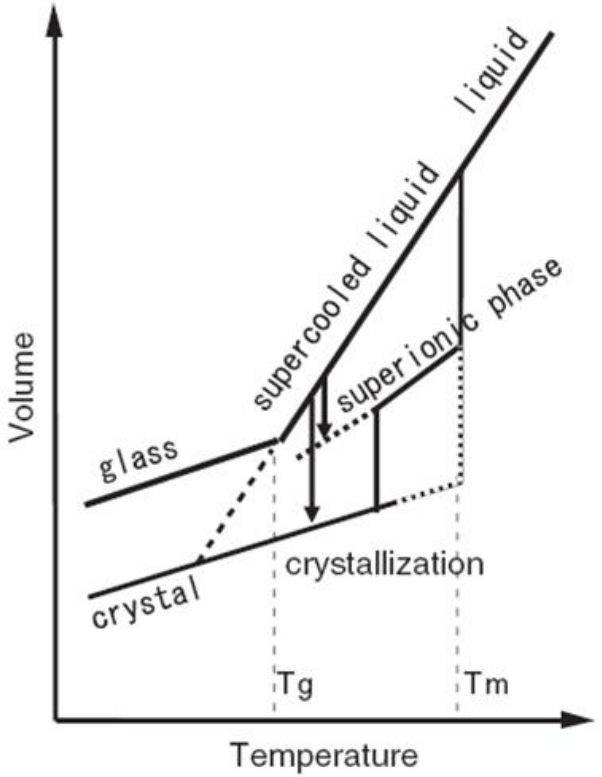

Heating of a glass beyond the glass-transition temperature usually results in crystallization with decreased conductivity.

However, if the corresponding crystal has a high-temperature superionic phase, crystallization tends to lead to the formation of the high-temperature superionic phase as a metastable phase.

Inclusion of high-temperature, superionic, crystalline phases, with larger volumes and are metastable at room temperature (RT).

α-AgI (by suppression of the α ➔ β transformation) in 82AgI -13.5Ag_2O-4.5B_2O_3

T. Saito, J. Electrochem. Soc. 143 (1996) 687–691
M. Tatsumisago, J. Phys. Chem. 98 (1994) 2005–2007

$Li_7P_3S_{11}$ in 70Li_2S-30P_2S_5 glass

M. Tatsumisago, Solid State Ionics. 225, (2012) 342–345

Na_3PS_4

A. Hayashi, Nature Communications 3 (2012) Article number: 856, 1-5.

M. Tatsumisago & A. Hayashi, Solid State Ionics, Volume 225, 4 October 2012, Pages 342-345
Superionic glasses and glass–ceramics in the Li_2S–P_2S_5 system for all-solid-state lithium secondary batteries

Stable crystalline phase with lower Grain-Boundary resistance

$Li_{1.5}Al_{0.5}Ti_{1.5}(PO_4)_3$ $\sigma_{glass\text{-}ceramic}$ about 1×10^{-4} Scm^{-1} > $\sigma_{ceramic}$ 6×10^{-5} Scm^{-1} > σ_{glass} 10^{-10} -10^{-8} Scm^{-1}

$Li_2CO_3 + Al_2O_3 + GeO_2 + NH_4H_2PO_4$

$\Rightarrow Li_2O \cdot 6.17\,Al_2O_3 \cdot 37.04\,GeO_2 \cdot 37.04\,P_2O_5$ glass (mol%)]

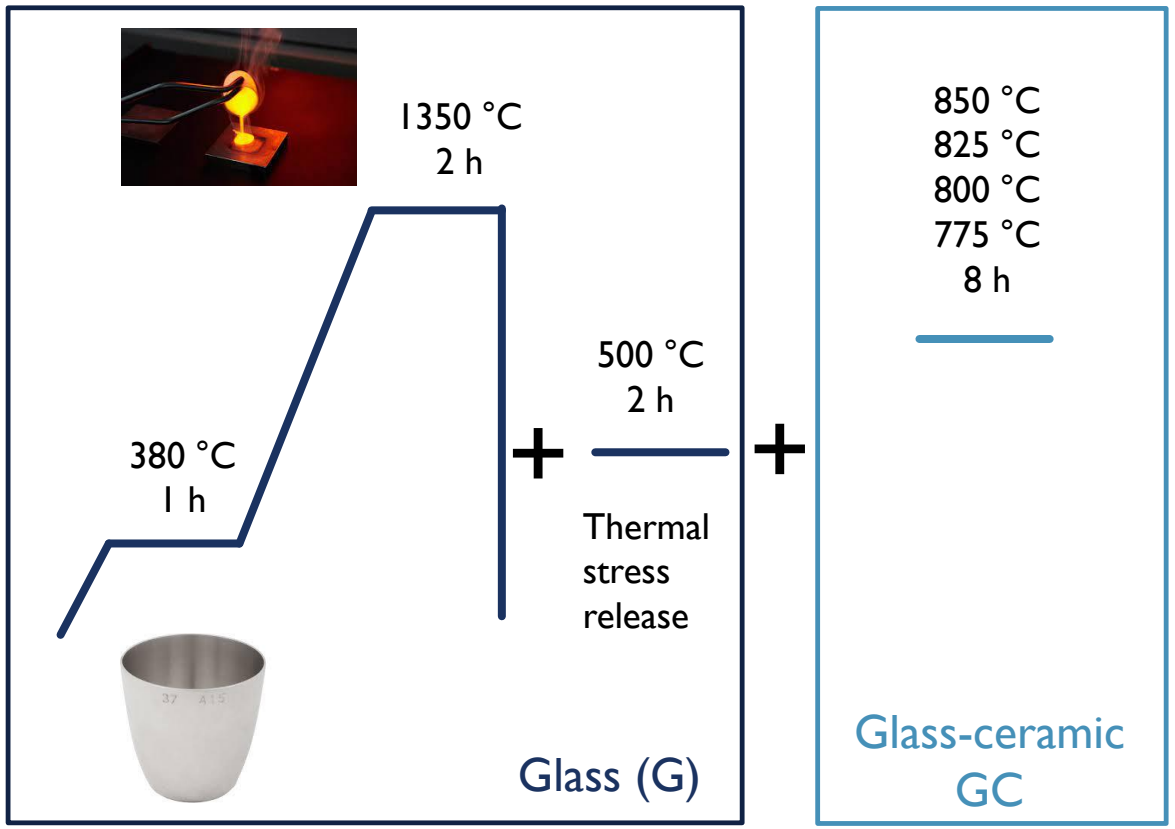

S. Duan, Journal of Power Sources, Volume 449, 15 February 2020, 227574

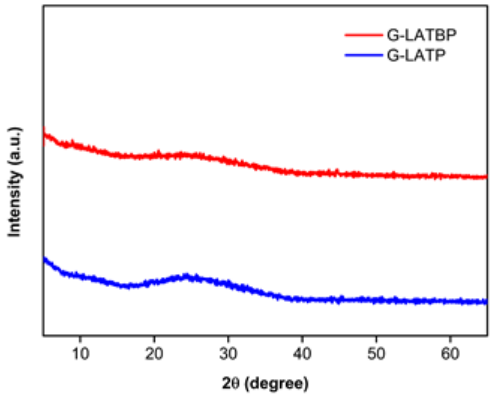

$Li_{1.3}Al_{0.2}B_{0.1}Ti_{1.7}(PO_4)_3$ (LATBP)

$Li_{1.3}Al_{0.3}Ti_{1.7}(PO_4)_3$ (LATP)

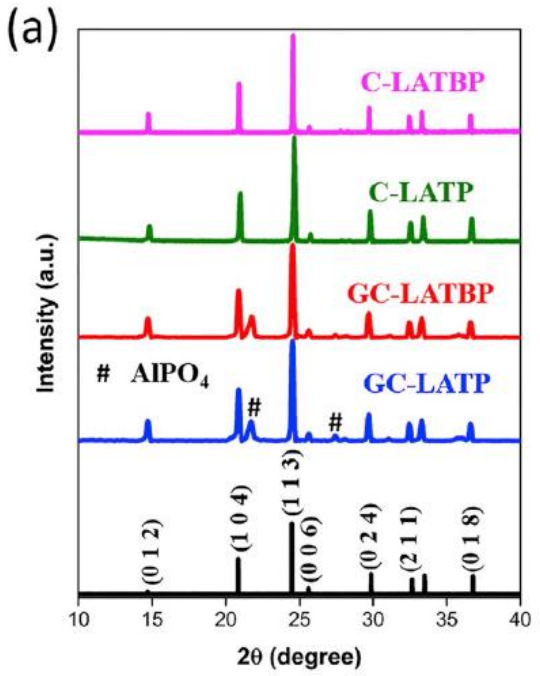

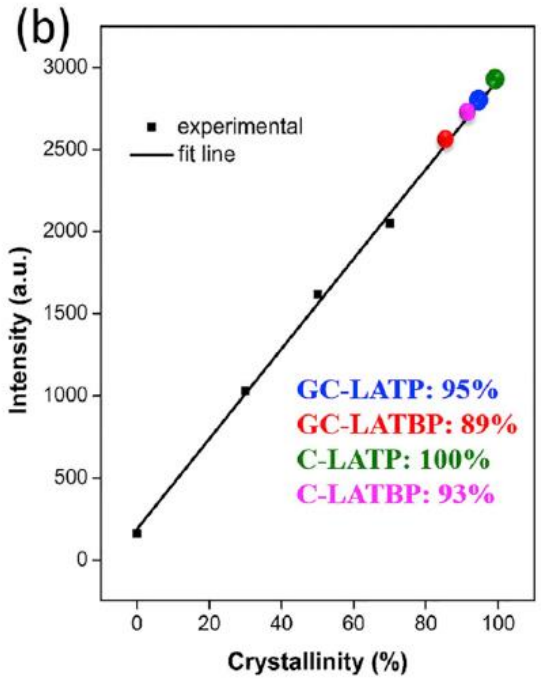

Stable crystalline phase with lower Grain-Boundary resistance

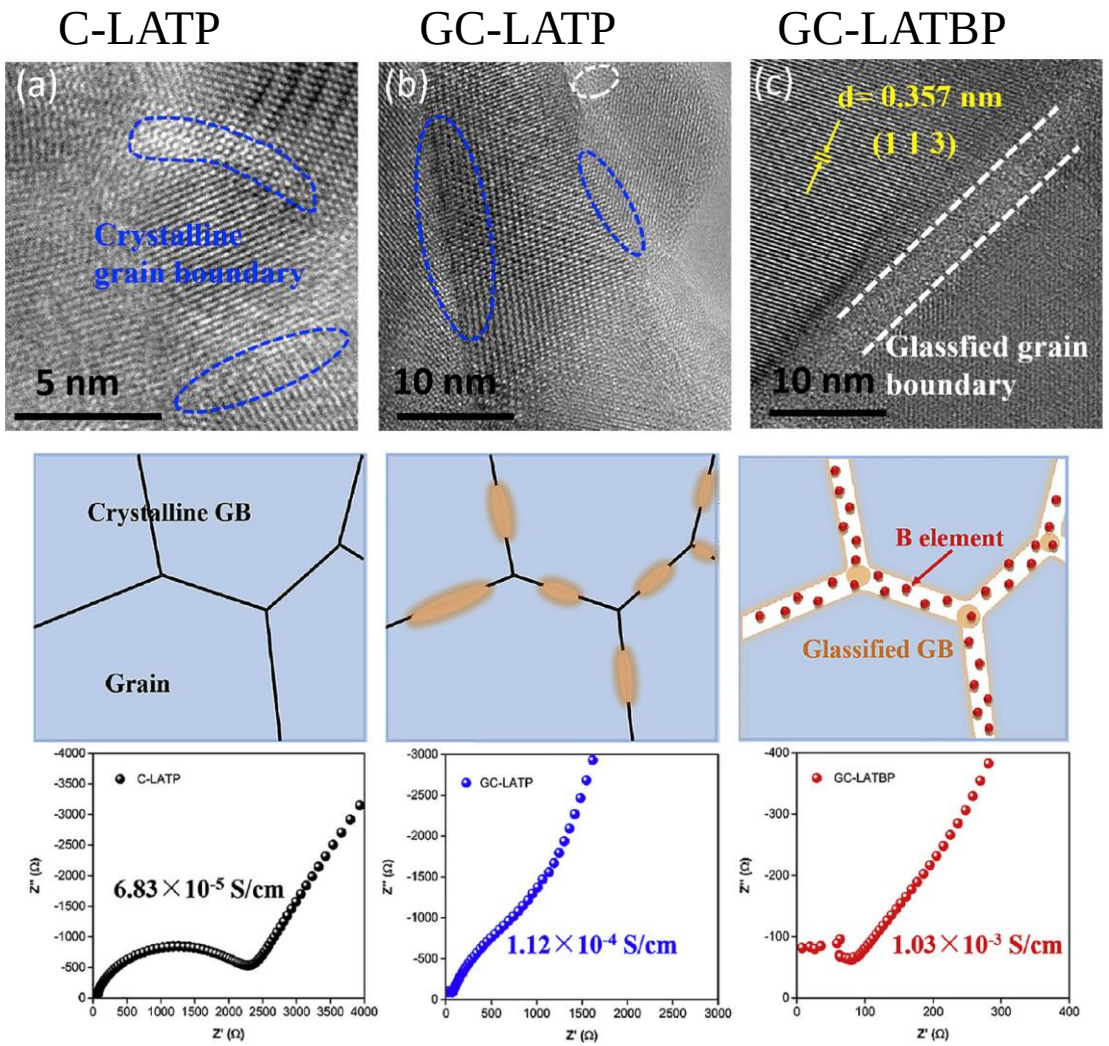

S. Duan, Journal of Power Sources, Volume 449, 15 February 2020, 227574

Arrhenius plots of bulk conductivity

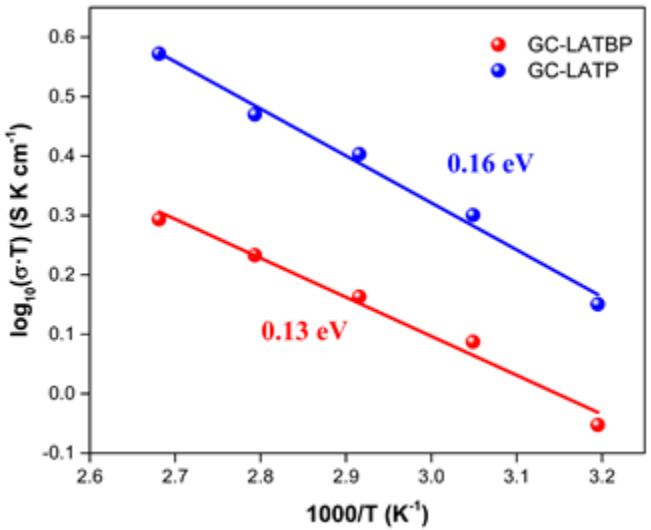

$$\sigma . T = A . exp\left(-\frac{E_a}{k_B . T}\right)$$

T Absolute temperature
k Boltzmann constant
A Pre-exponential factor

- inhomogeneous distribution of boron and glassified grain boundaries
  ⇒ reduces interfacial resistance at grain boundaries with little effect on bulk resistance,
- grain boundary resistance of ceramics, on the other hand, is increased by boron

⇒ higher conductivity in glass-ceramics, while boron can relax their grain boundaries even further.

From glass to glass-ceramic: $70Li_2S$-$30P_sS_5$

Mechanical milling
$Li_2S+P_2S_5$

Al_2O_3 balls and pot
20 h at 370 rpm

DTA curve for the $70Li_2S \cdot 30P_2S_5$ (mol %) mechanically milled sample.

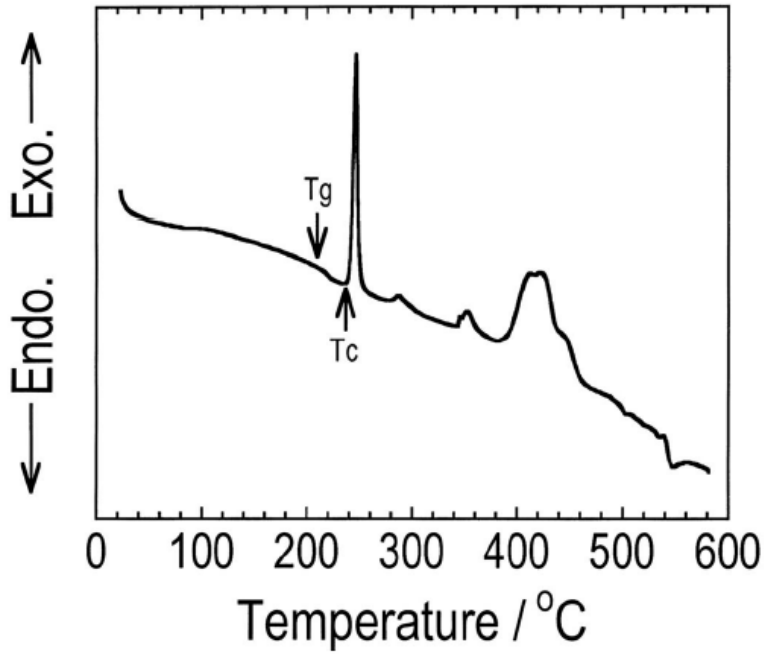

- Glass transition Tg is observed at around 210°C
- Crystallization Tc is observed at 240°C,

Temperature dependences of the conductivities for $xLi_2S \cdot 100 - xP_2S_5$ mol % glass-ceramics with several compositions (Tc <T < 260°C)

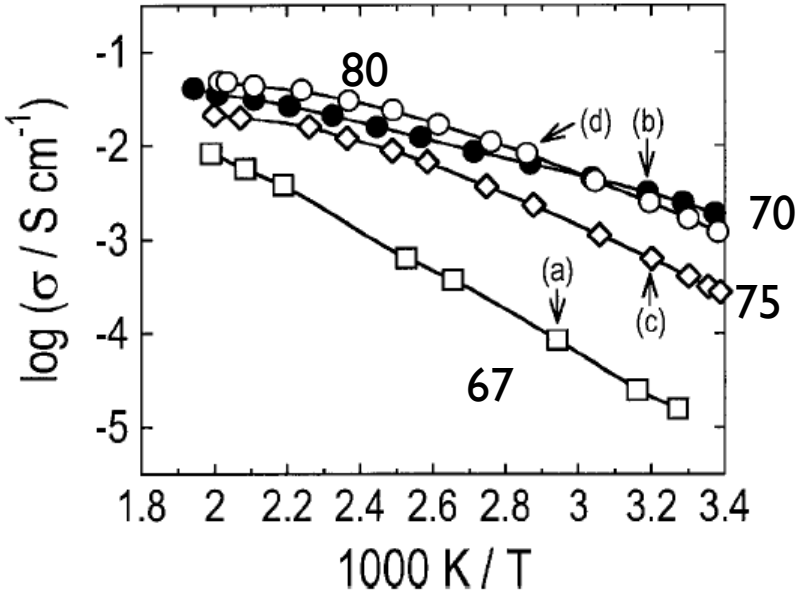

- $Li_4P_2S_6$ crystal with x = 67 mol, 10^{-6} $S.cm^{-1}$
- Highest conductivities with x = 70 and 80 : glass-ceramic thio-LISICON II or III analog, 10^{-4} $S\ cm^{-1}$.

F. Mizuno, Electrochemical and Solid-State Letters, 8 (11) A603-A606 (2005)
New Lithium-Ion Conducting Crystal Obtained by
Crystallization of the Li_2S–P_2S_5 Glasses

Glass-ceramic and superionic phase: $Li_7P_3S_{11}$

XRD patterns of the $70Li_2S \cdot 30P_2S_5$ (mol %) glass-ceramics obtained by heating the glasses

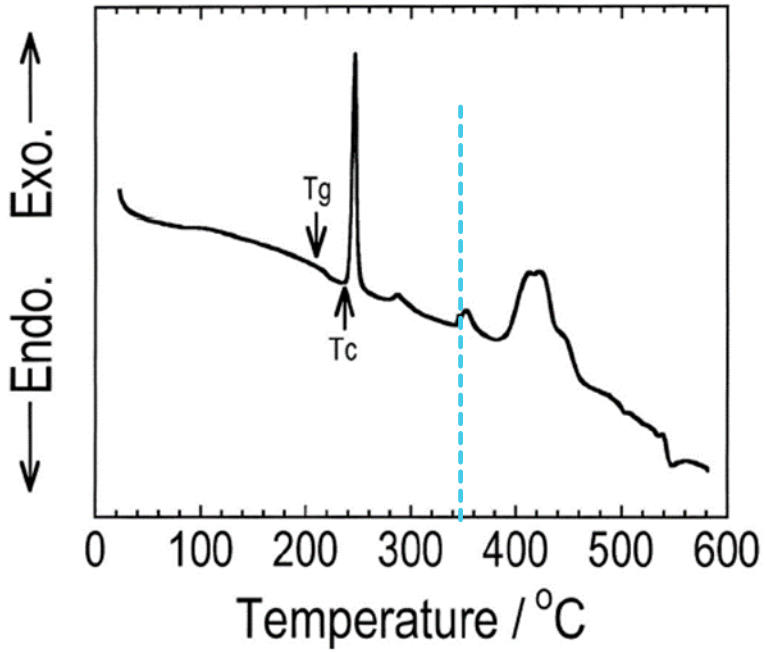

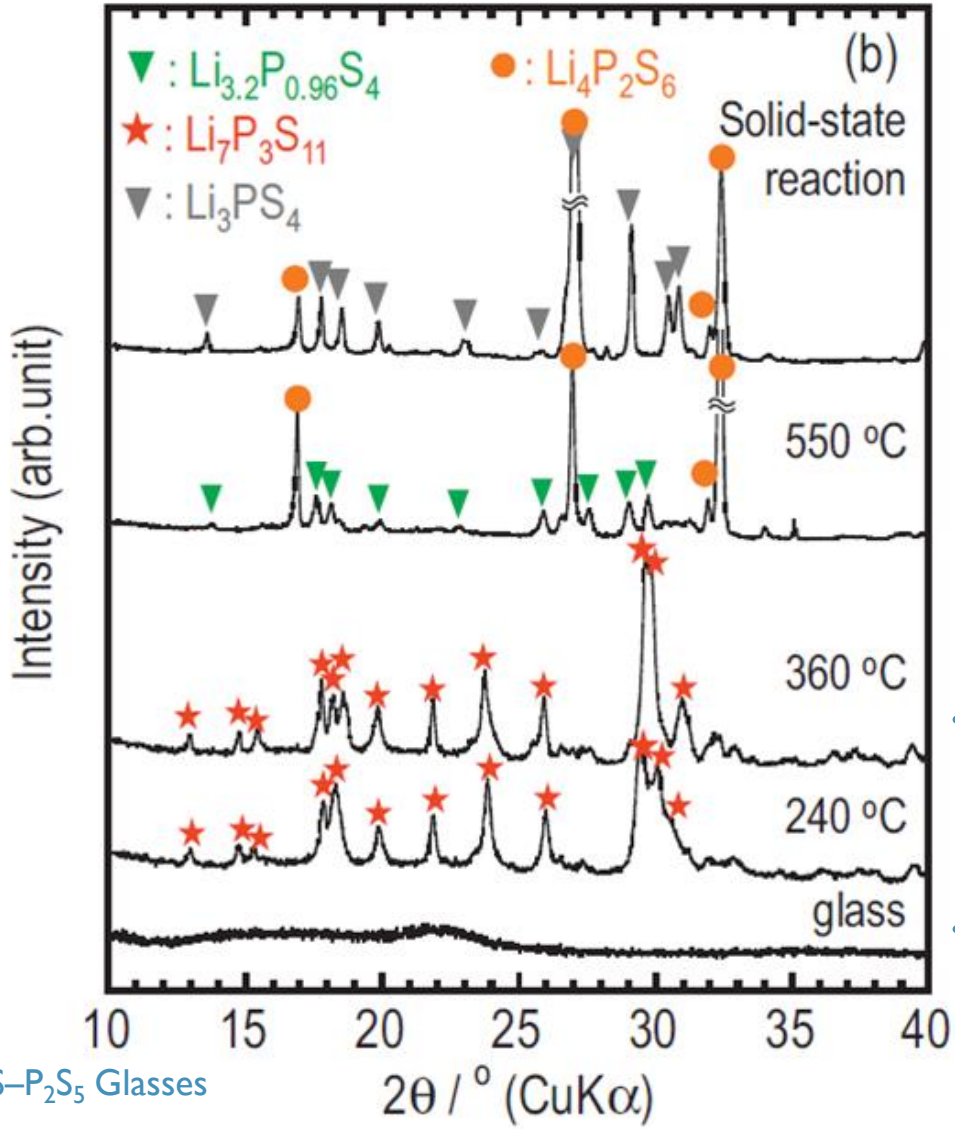

highly conductive new crystalline phase

F. Mizuno, Electrochemical and Solid-State Letters, 8 (11) A603-A606 (2005)
New Lithium-Ion Conducting Crystal Obtained by Crystallization of the Li_2S–P_2S_5 Glasses

Glass-ceramic and superionic phase: $Li_7P_3S_{11}$

$70Li_2S \cdot 30P_2S_5$ (mol%) glass

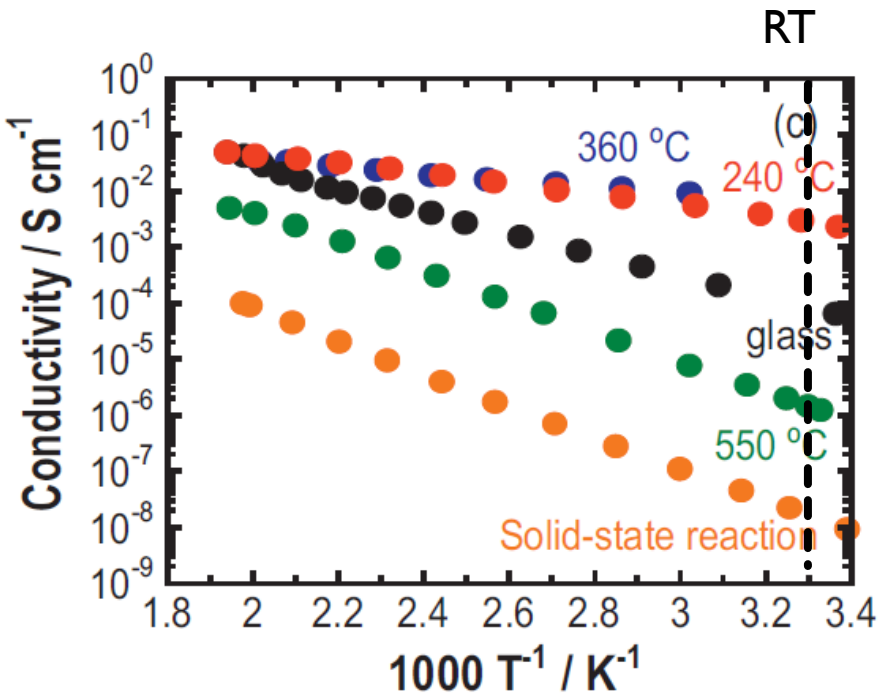

temperature dependence of conductivities
for the $70Li_2S \cdot 30P_2S_5$ (mol%) glass and glass–ceramics

highly conductive new crystalline phase

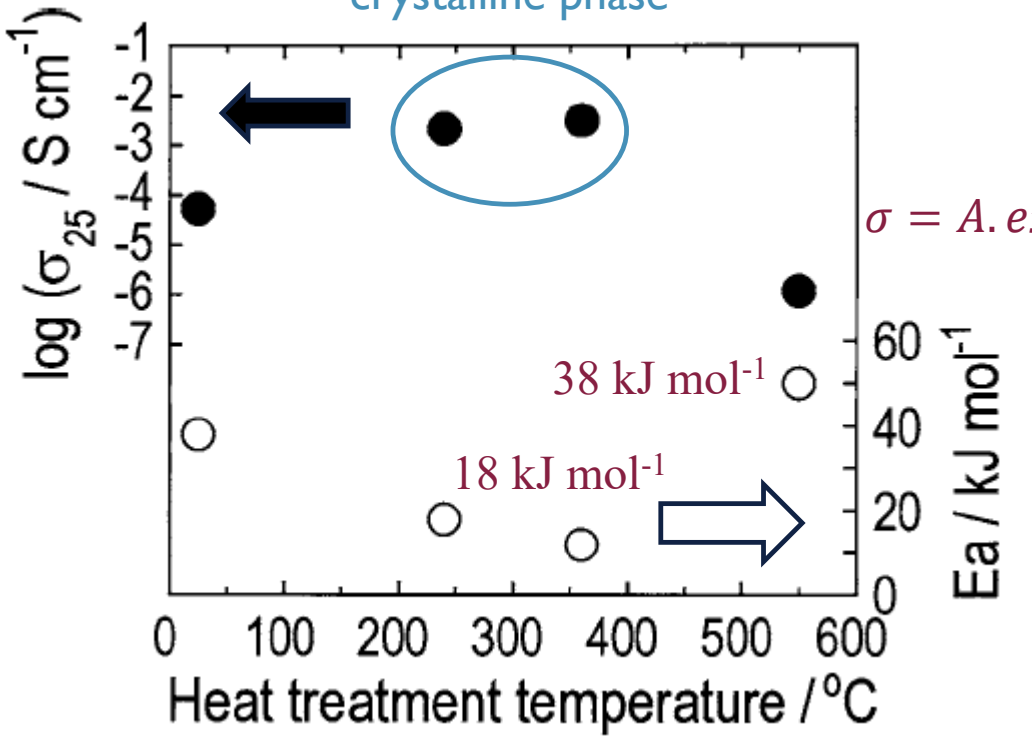

$$\sigma = A.exp\left(-\frac{E_a}{k.T}\right)$$

BM	glass	$\sigma_{ion(RT)} = 5.4 \times 10^{-5}$ S cm^{-1}
240 °C	glass-ceramic	$\sigma_{ion(RT)} = 2.2 \times 10^{-3}$ S cm^{-1}
360 °C	glass-ceramic	$\sigma_{ion(RT)} = 3.2 \times 10^{-3}$ S cm^{-1}
550 °C	Thio LISICON + $Li_4P_2S_6$	$\sigma_{ion(RT)} = 1.1 \times 10^{-6}$ S cm^{-1}
Solid state : Li_3PS_4 + $Li_4P_2S_6$		$\sigma_{ion(RT)} = 10^{-8}$ S cm^{-1}

M. Tatsumisago, Journal of Asian Ceramic Societies 1 (2013) 17–25

Glass-ceramic and superionic phase: $Li_7P_3S_{11}$

Structural model of superionic $Li_7P_3S_{11}$ crystal

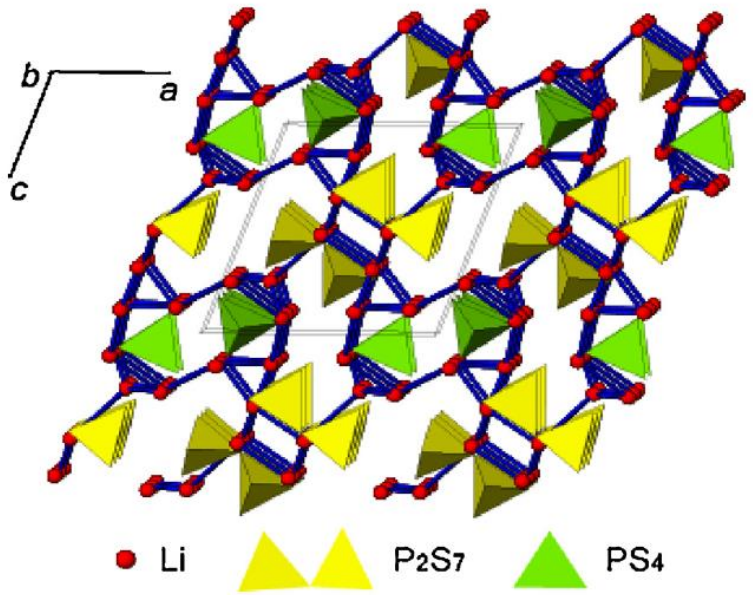

Li–Li correlations (solid blue lines) within 4 ˚A

- Triclinic cell (space group P−1)
- Both PS_4^{3-} tetrahedral and $P_2S_7^{4-}$ ditetrahedral ions are contained in the structure and Li^+ ions are situated between them.
- The crystal structure is completely different from other superionic conducting crystals such as $Li_{3.25}Ge_{0.25}P_{0.75}S_4$ and $Li_{10}GeP_2S_{12}$, which are composed of only tetrahedral ions (PS_4^{3-} and GeS_4^{3-}).
- Favorable Li^+ conduction path is presumably close to the Li–Li chains.

M. Tatsumisago, Journal of Asian Ceramic Societies 1 (2013) 17–25 synchrotron X-ray powder diffraction pattern.

Scalability of ball-milling process?
Compatibility with battery fabrication process?

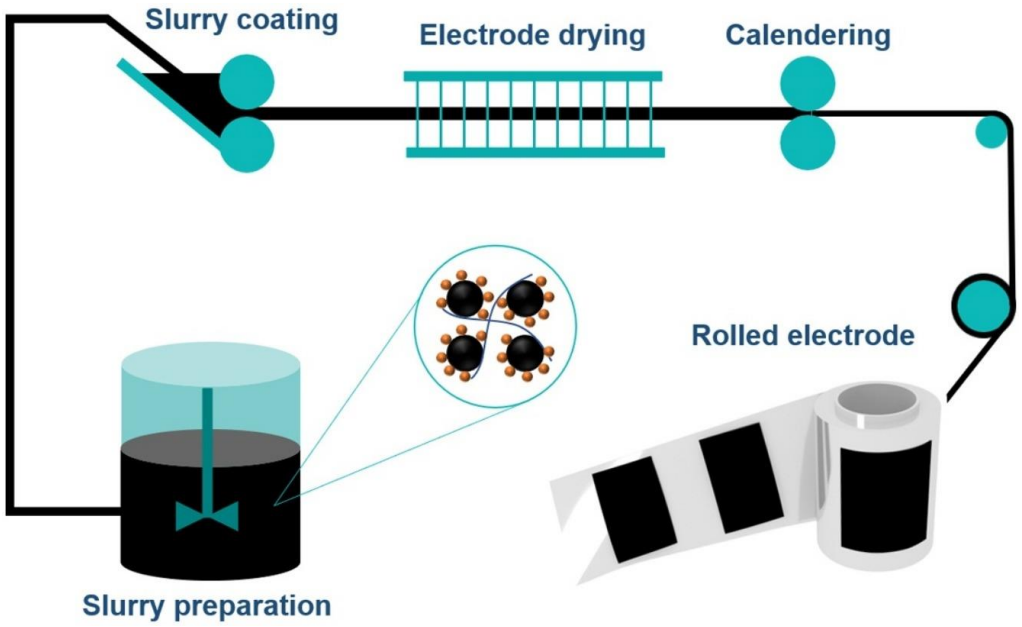

H. Liu, Particuology 57 (2021) 56–71

Assembling by wet-slurry process

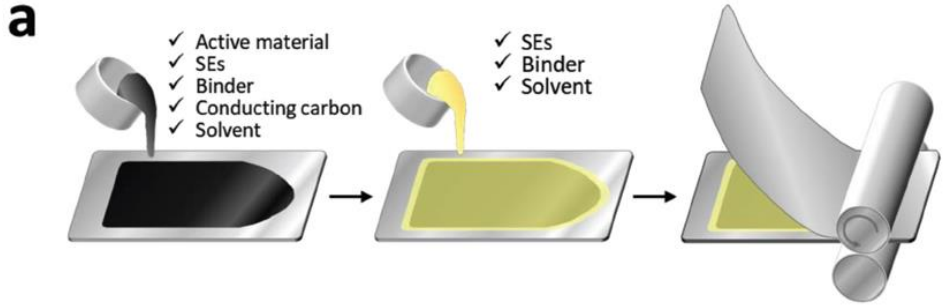

Application of solution-Processable SE for ASSB: impregnation

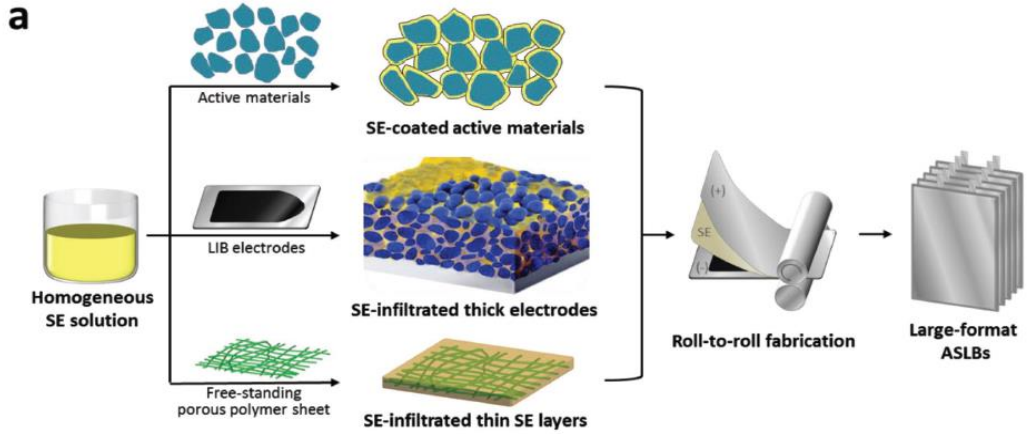

K. H. Park *et al.*, Adv. Energy Mater. 2018, 8, 1800035

Solvent assisted synthesis

Solvent Assisted Synthesis of GC-$Li_7P_3S_{11}$

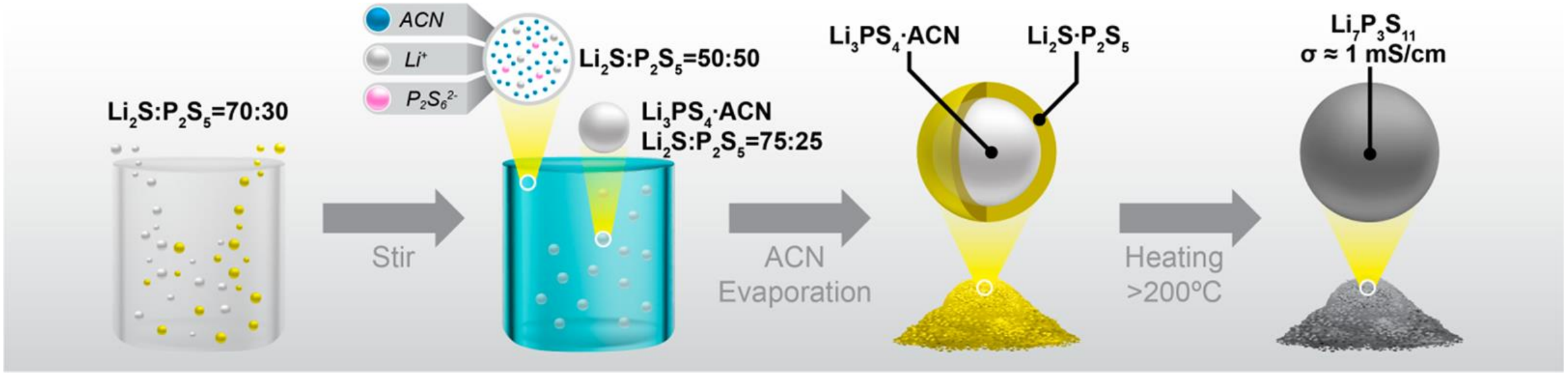

- Mixture of Li_3PS_4 and 50:50 Li_2S-P_2S_5 powder obtained after drying ACN
- Formation of GC-$Li_7P_3S_{11}$ after heating
- Formation of GC-$Li_7P_3S_{11}$ requires T > 260 °C

Wang et al., Chem. Mater. 30 (3), 990, 2018

Solvent Assisted Synthesis of GC-$Li_7P_3S_{11}$

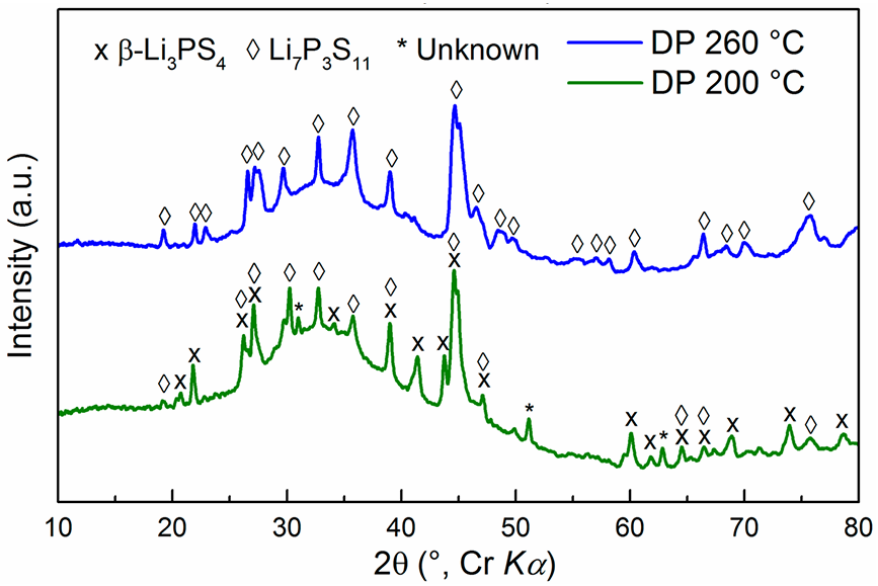

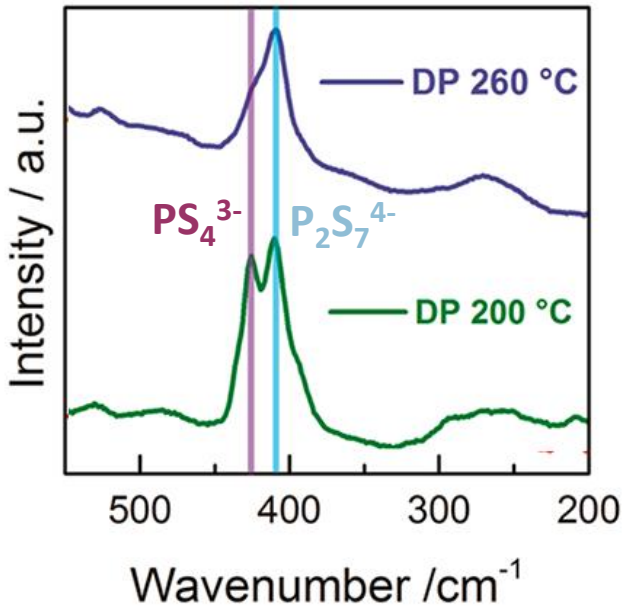

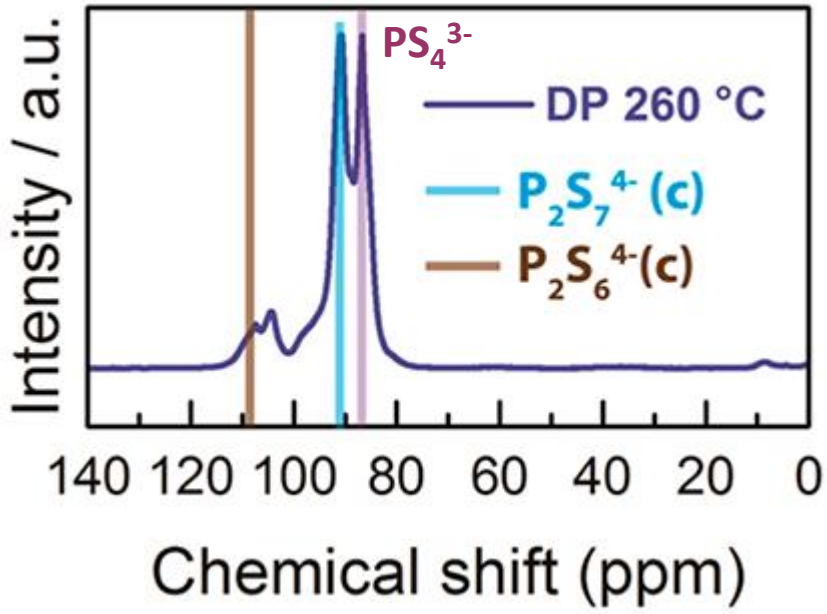

- Below 260 °C, crystallization of β-Li_3PS_4
- T > 260 °C required for complete stoichiometric reaction and $Li_7P_3S_{11}$ formation

Wang et al., Chem. Mater. 30 (3), 990, 2018

Thermal stability of $Li_7P_3S_{11}$

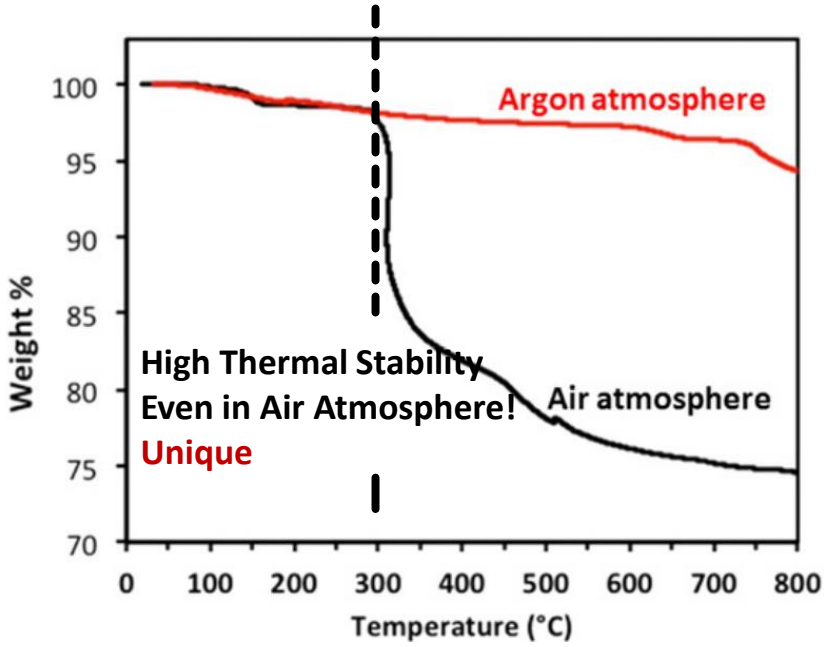

Thermally Stable unlike the Other LPS

$$Li_7P_3S_{11} \rightarrow Li_4P_2S_6 + Li_3PS_4 + \frac{1}{8}S_8$$ **(at 280 °C, inert atm.)***

$$Li_3PS_4 \leftrightarrow \frac{1}{2}S + \frac{1}{2}Li_2S + \frac{1}{2}Li_4P_2S_6$$ **(by DFT)****

Hood et al., Solid State Ion., 61, 2016
*Busche et al., Chem, Mater., 28 (17), 6152, 2016
**Chen et al., Phys. Chem. Chem. Phys., 17, 16494, 2015

27

Electrochemical stability of $Li_7P_3S_{11}$

Cyclic voltammogram

Stainless steel- GC $Li_7P_3S_{11}$–Li metal

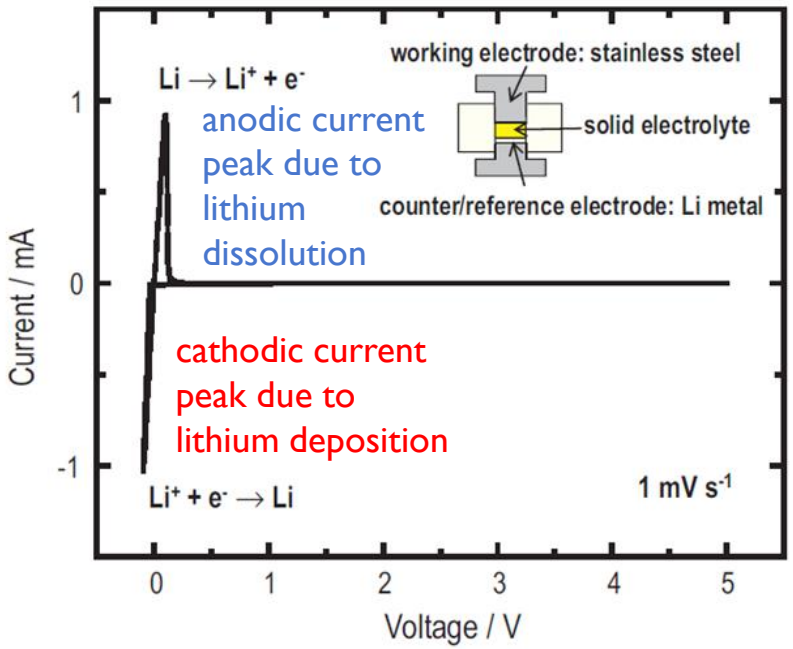

- No large current peak except Li peaks over the whole range from −0.1 V to 5.0 V.

⇒ Wide electrochemical window of over 5 V

⇒ Good compatibility with lithium metal

M. Tatsumisago, Journal of Asian Ceramic Societies 1 (2013) 17–25

Potentiostatic Cycling

Li-GC $Li_7P_3S_{11}$-Li symmetric cell

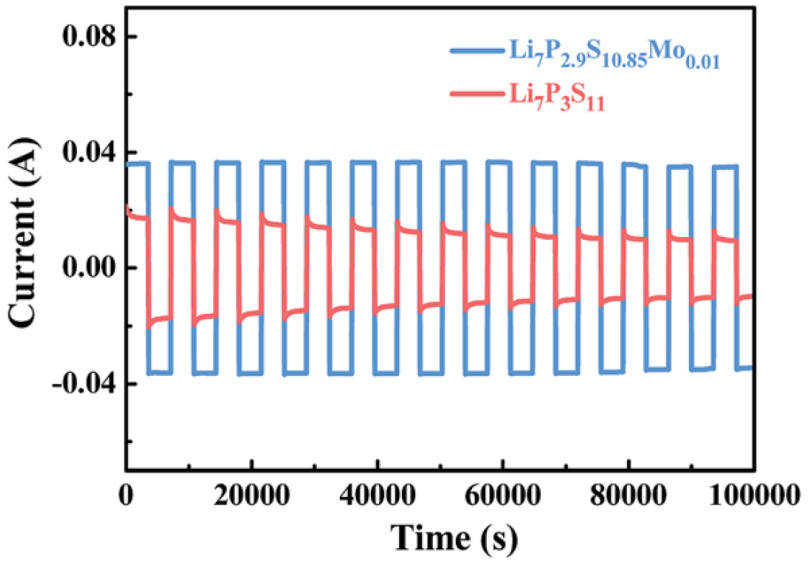

Decreasing current over time

- Increasing resistance
- Reaction at interfaces

Seino et al., J. Mater. Chem. A, 3, 2756, 2015 / Xu et al., J. Mater. Chem. A, 5, 2829, 2017

Galvanostatic Cycling

Li metal - GC $Li_7P_3S_{11}$ - (S & C & GC $Li_7P_3S_{11}$)

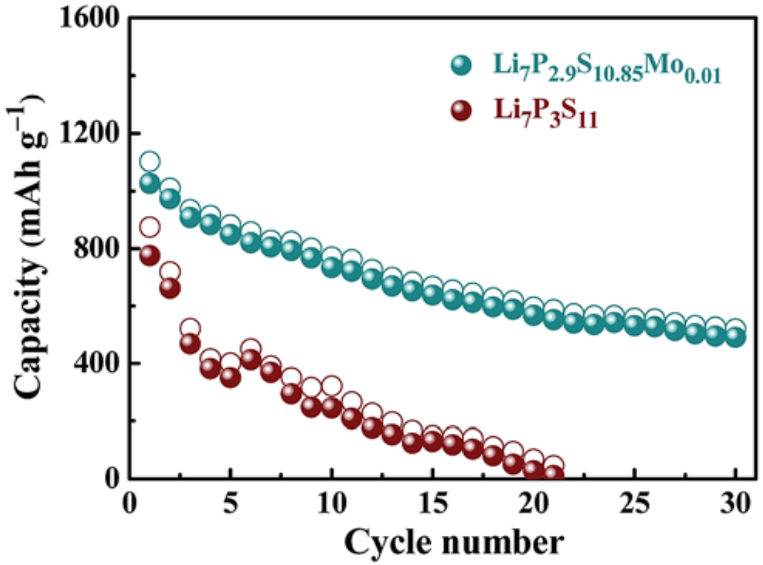

Battery dies fast due to side reactions

⇒ **Limited electrochemical stability**

Improvement of the stability of sulfide electrolytes

- substitution engineering of O to S
- replacement of P and S elements with congeners, such as more polarizable Sb and more stable O (theory of hard and soft acid−base (HSAB))

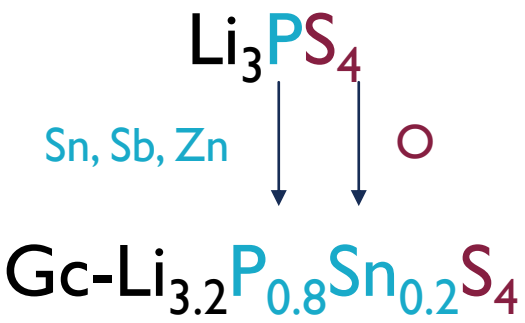

B.H. Zhao, Adv. Mater. 2021, 33, 2006577

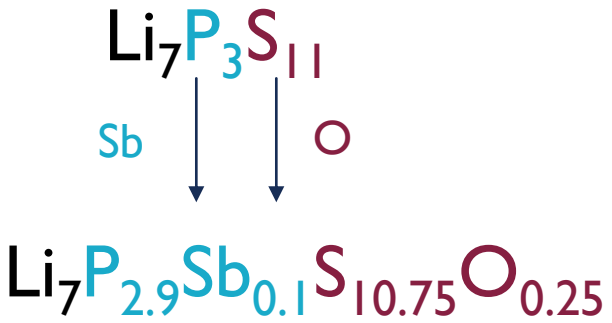

B.H. Zhao, ACS Appl. Mater. Interfaces 2021, 13, 34477−34485

Goal
- To increase the air-stability
- To improve the Li metal compatibility

Improvement of the stability of sulfide electrolytes

$Li_7P_3S_{11}$

Sb ↓ ↓ O

$Li_7P_{2.9}Sb_{0.1}S_{10.75}O_{0.25}$

- substitution engineering of O to S
- replacement of P and S elements with congeners, such as more polarizable Sb and more stable O (theory of hard and soft acid−base (HSAB))

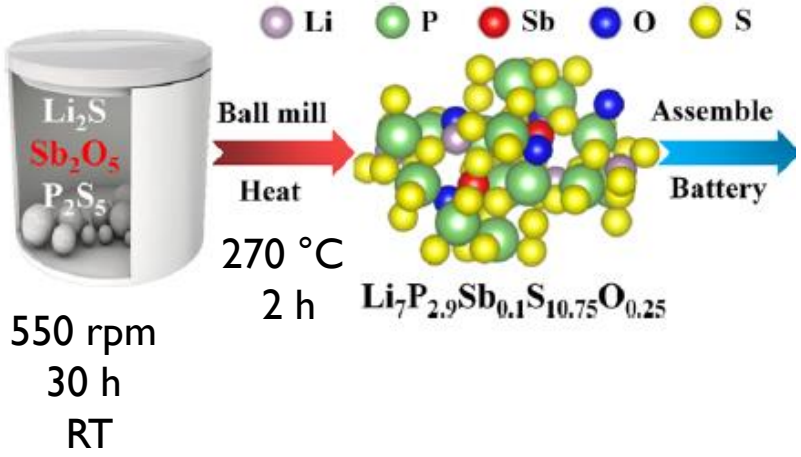

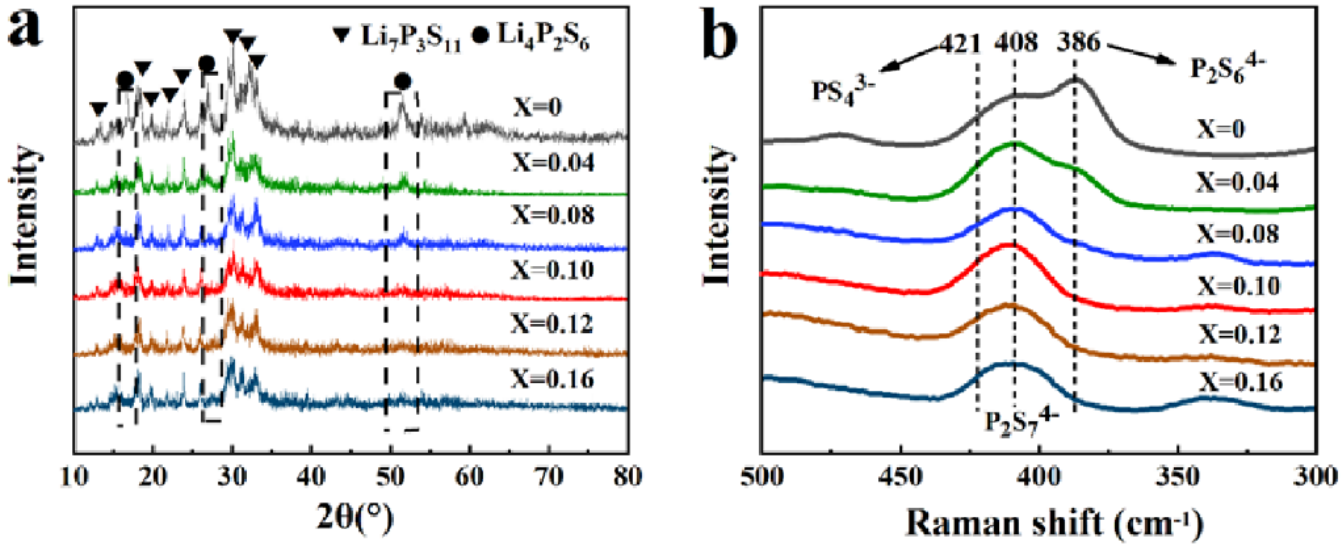

- Pure $Li_7P_3S_7$ for x ≥ 0,10
- no diffraction peaks of Sb_2O_5

⇒ Sb and O successfully incorporated

B.H. Zhao, ACS Appl. Mater. Interfaces 2021, 13, 34477−34485
Congener Substitution Reinforced $Li_7P_{2.9}Sb_{0.1}S_{10.75}O_{0.25}$ Glass-Ceramic Electrolytes for All-Solid-State Lithium−Sulfur Batteries

Improvement of the stability of sulfide electrolytes

Nyquist plots
SS/solid-state electrolyte/SS cells

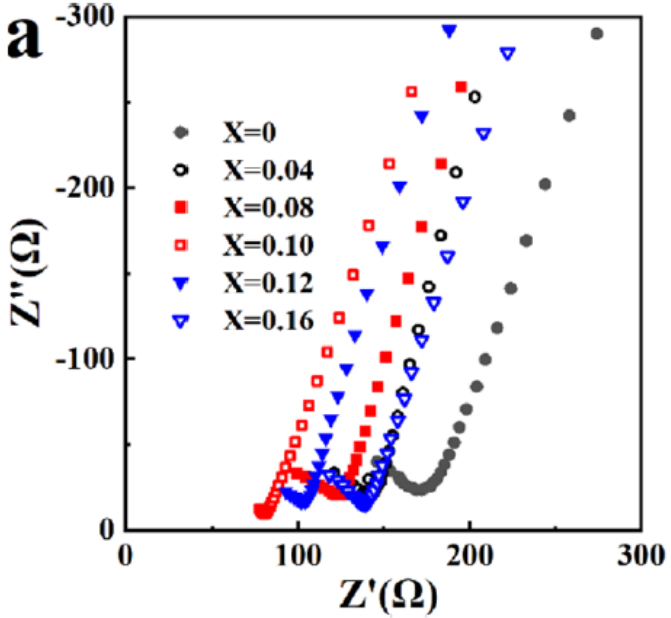

Arrhenius plots of ionic conductivity

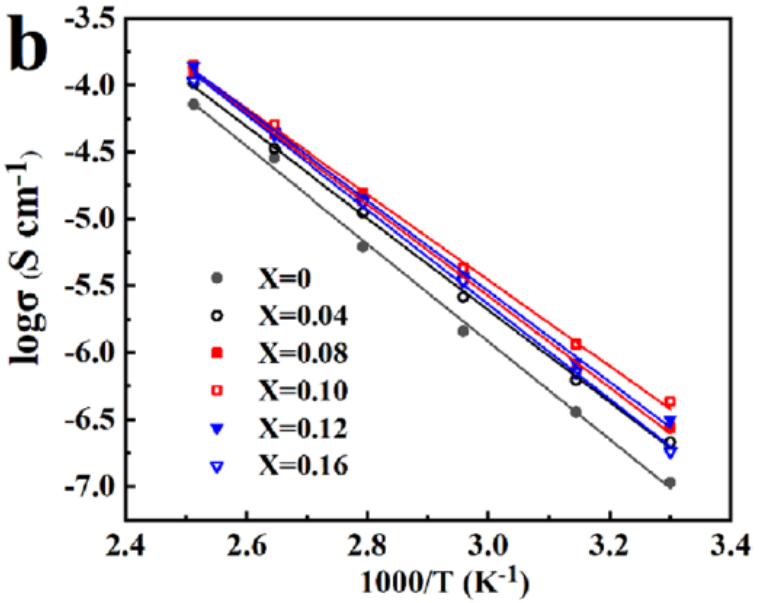

- σ ↑ from x=0 to x=0.1 then ↓
- σion for 0=0.10 is 2.2 times higher than that of the pristine Li7P3S11

- Smallest activation energy Ea of x = 0.10, while the pristine
- $Li_7P_3S_{11}$ electrolyte presents the largest Ea value

B.H. Zhao, ACS Appl. Mater. Interfaces 2021, 13, 34477−34485

$Li_7P_3S_{11}$

Sb ↓ ↓ O

$Li_7P_{2.9}Sb_{0.1}S_{10.75}O_{0.25}$

$Li_7P_{3-x}Sb_xS_{11-2.5x}O_{2.5x}$
(x = 0, 0.04, 0.08, 0.1, 0.12, and 0.16)

$$\sigma = A.\exp\left(-\frac{E_a}{k.T}\right)$$

X	conductivity (σ, S cm^{-1})	Ea (kJ mol^{-1})
0	7.26×10^{-4}	30.3
0.04	9.06×10^{-4}	28.5
0.08	1.04×10^{-3}	28.4
0.10	1.61×10^{-3}	26.6
0.12	1.22×10^{-3}	28.1
0.16	8.98×10^{-4}	29.3

Improvement of the stability of sulfide electrolytes

$Li_7P_3S_{11}$

Sb ↓ ↓ O

$Li_7P_{2.9}Sb_{0.1}S_{10.75}O_{0.25}$

$Li_7P_{3-x}Sb_xS_{11-2.5x}O_{2.5x}$
(x = 0, 0.04, 0.08, 0.1, 0.12, and 0.16)

Quantity of H_2S gas during air exposure

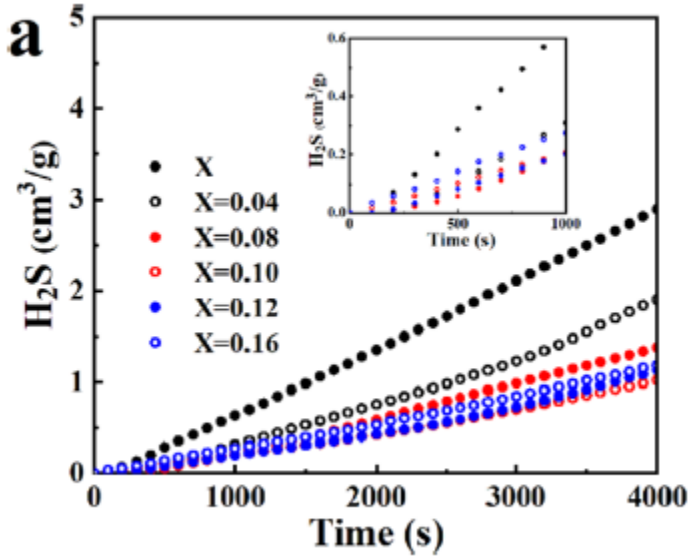

amount of H_2S gas generated after 4000 s air exposure tests.

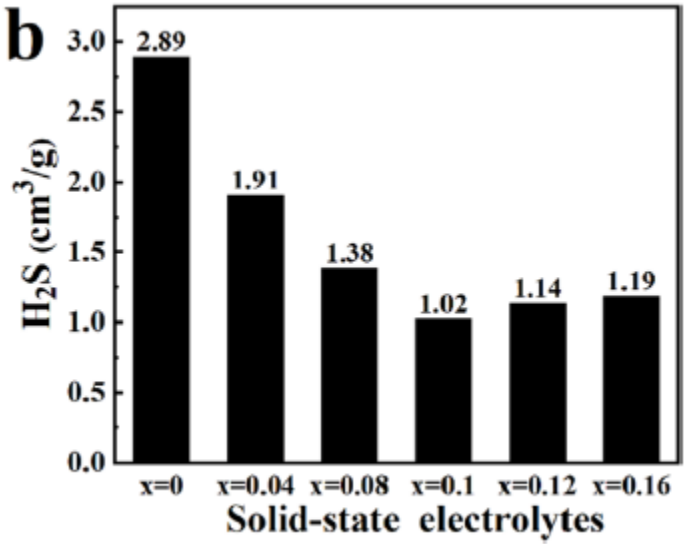

- Water in humid air can hydrolyze sulfide electrolyte and produce harmful H_2S, ultimately decomposing the electrolyte and reducing ionic conductivity.
- Amount of H_2S gas generated is gradually increased during the exposure.
- Pristine $Li_7P_3S_{11}$ electrolyte shows the fastest growing speed among all of the samples.

B.H. Zhao, ACS Appl. Mater. Interfaces 2021, 13, 34477−34485
Congener Substitution Reinforced $Li_7P_{2.9}Sb_{0.1}S_{10.75}O_{0.25}$ Glass-Ceramic Electrolytes for All-Solid-State Lithium−Sulfur Batteries

Improvement of the stability of sulfide electrolytes

Cyclic voltammograms of Li/solid electrolyte/Stainless steel cell

small peak at 2.3 V (vs Li/Li^+) attributed to the oxidative decomposition of $Li_7P_3S_{11}$

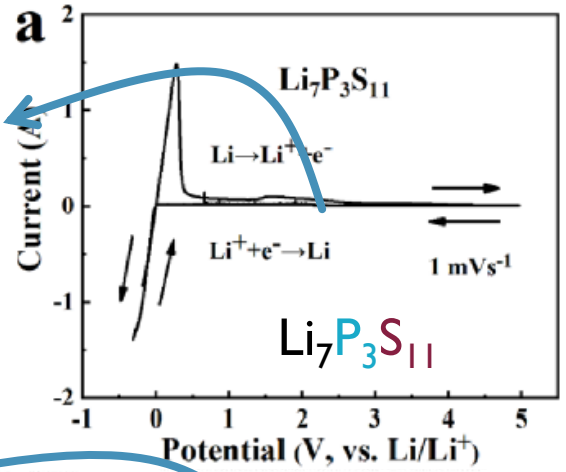

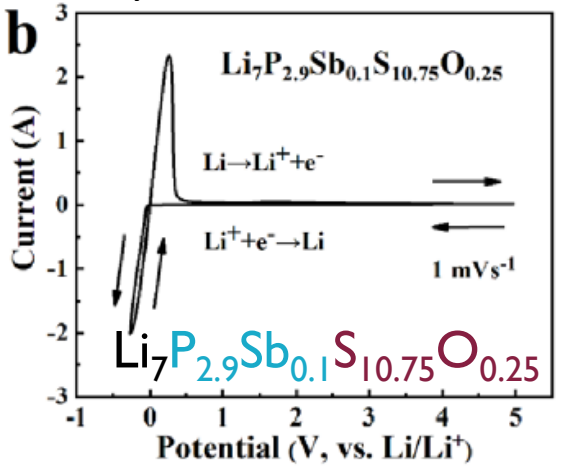

No other redox peaks except for the electrochemical deposition/dissolution of lithium
⇒ wide and stable electrochemical window of $Li_7P_{2.9}Sb_{0.1}S_{10.75}O_{0.25}$ up to 5.0 V vs Li/Li+.

Sudden drop of the voltage curve due to short circuit caused by the formation of lithium dendrites in the cell with $Li_7P_3S_{11}$

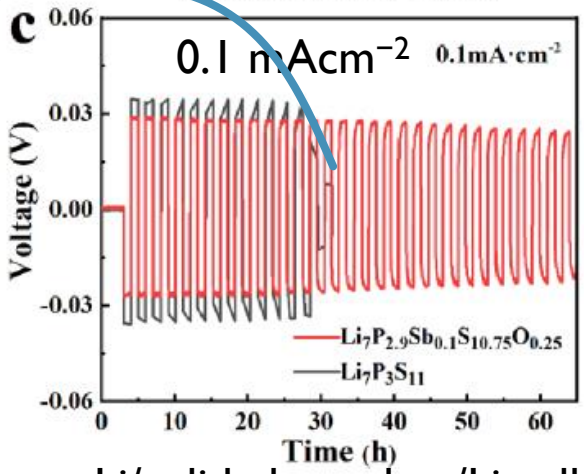

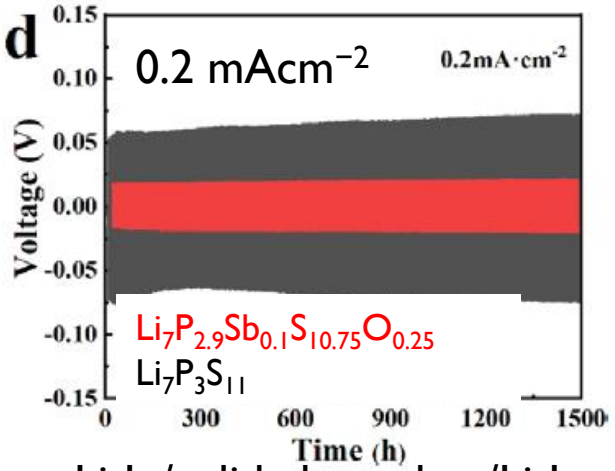

Steady stripping/plating behavior for for 62 h and lower overpotential (+0.023 and −0.022 V),
⇒ low interface resistance,
⇒ Good chemical/electrochemical stability of the $Li_7P_{2.9}Sb_{0.1}S_{10.75}O_{0.25}$
⇒ Suppression of lithium dendrites.

Li/solid electrolyte/Li cells Li-In/solid electrolyte/Li-In cells

Galvanostatic charge/discharge curves of Li/solid electrolyte/Li cells

B.H. Zhao, ACS Appl. Mater. Interfaces 2021, 13, 34477−34485

Na ion conductors

- Na_3PS_4 glass-ceramic higher conductivity than sulphide glasses and a $Na_3Zr_2Si_2PO_{12}$ NASICON crystal.
- β-alumina (consisting of β and β″ phases) and a NASICON-type crystal (Ceramatec) have a higher conductivity of 10^{-3} S cm^{-1} at RT but sintering at a high temperature of 1,800 °C needed to reduce the grain-boundary resistance for β-alumina.
- Conductivity of the Na_3PS_4 glass-ceramic electrolyte one order of magnitude lower than that of sintered β-alumina and the NASICON-type crystal but good electrode–electrolyte contact by simple cold pressing.

Conductivities of several Na^+ ion conductors

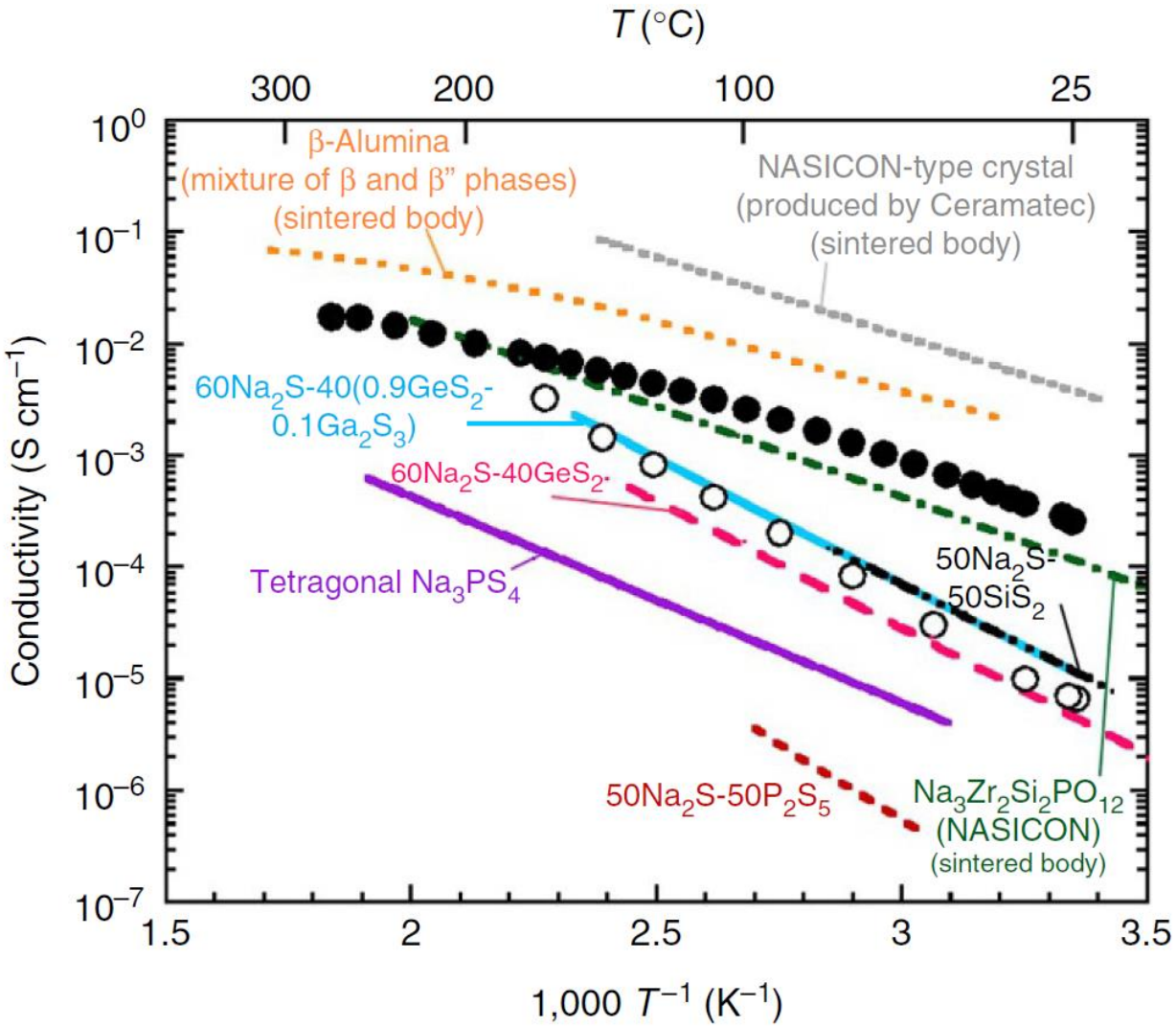

Na_3PS_4 glass-ceramic prepared at 270 °C (●)

Na_3PS_4 glass (○)

A. Hayashi, K. Noi, A. Sakuda, M. Tatsumisago, Nature Communications 3 (2012) Article number: 856, 1-5.

Na ion conductors

Glass (ball-milling)

Glass Ceramic 270 °C cubic

Glass Ceramic 420 °C tetragonal

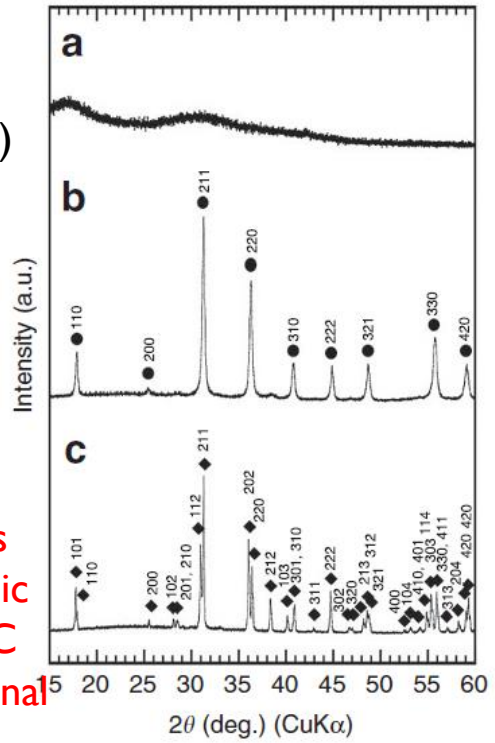

halo pattern in its X-ray diffraction (XRD) pattern

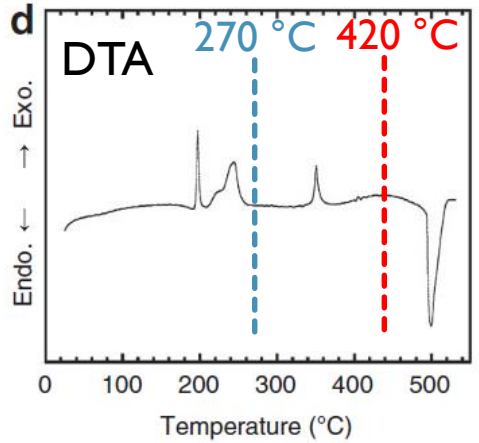

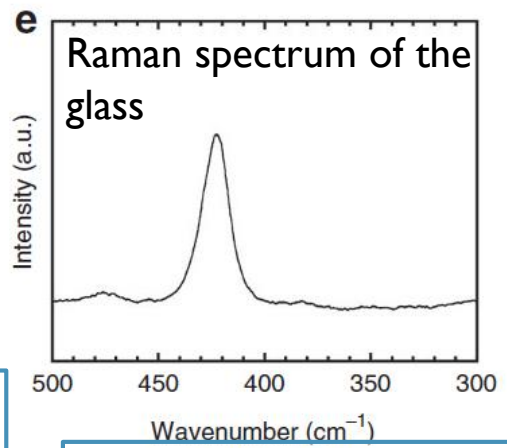

single band at 420 cm^{-1},
⇒ ortho-thiophosphate ion (PS_4^{3-})

A. Hayashi, K. Noi, A. Sakuda, M. Tatsumisago, Nature Communications 3 (2012) Article number: 856, 1-5.

Crystal structure of Na_3PS_4 projected in the (010) plane

Cubic
High-temperature phase

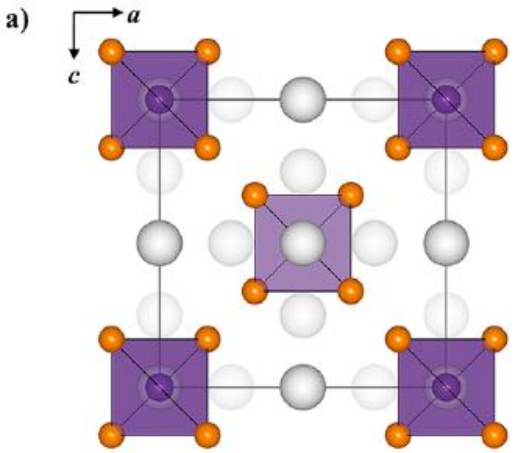

(Defective) **Cubic structure**

$I\bar{4}3m$

S (8*c*), Na (6*b*, 12*d*), P (2*a*)

- No occupancy of the 12d positions)
- PS_4^{3-} tetrahedra in a body centered lattice.

Tetragonal
Low-temperature phase

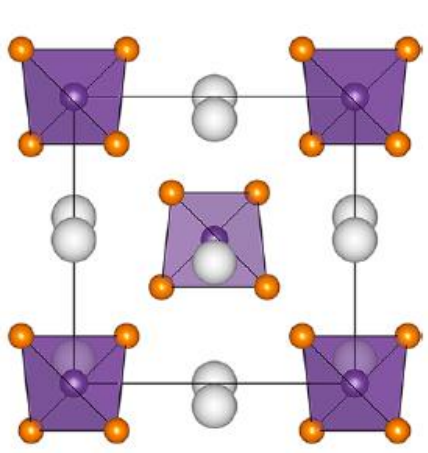

Tetragonal structure

$P\bar{4}2_1c$

S (8*e*), Na (4*d*, 2*a*), P (2*a*)

- minor rotation of the tetrahedra
⇒ splitting of the Na positions
⇒ elongation of the c-lattice parameter.

T. Krauskopf, Inorg. Chem. 2018, 57, 4739−4744

Na ion conductors

Impedance plots

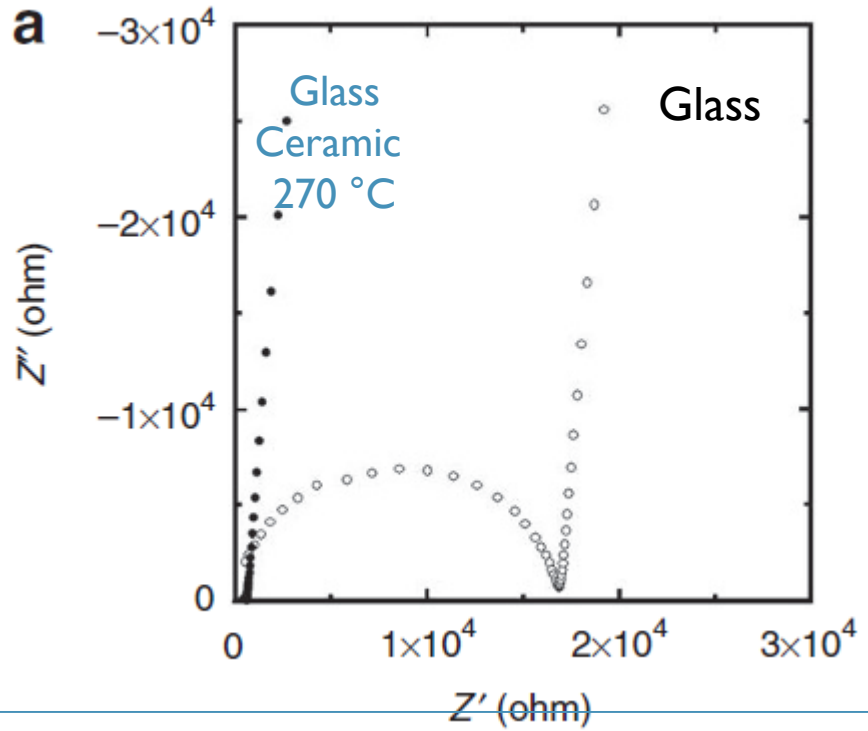

Glass: semicircle and a spike in the low-frequency region
⇒ typical ionic conductor.
⇒ total conductivity includes the bulk-grain and grain-boundary resistances
Glass-ceramic: resistance of the pellet decreases by a factor of 30 on crystallization

Cross-sectional SEM images

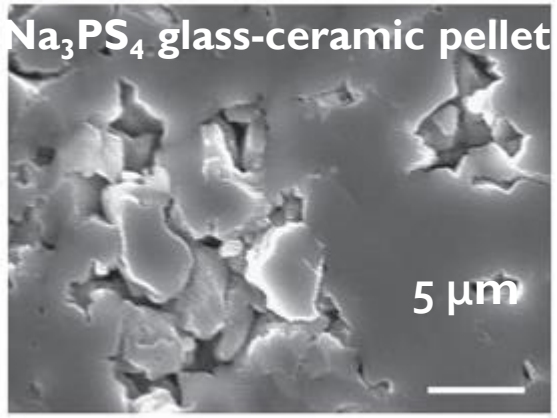

Intimate contacts among particles achieved in the Na_3PS_4 glass-ceramic pellet

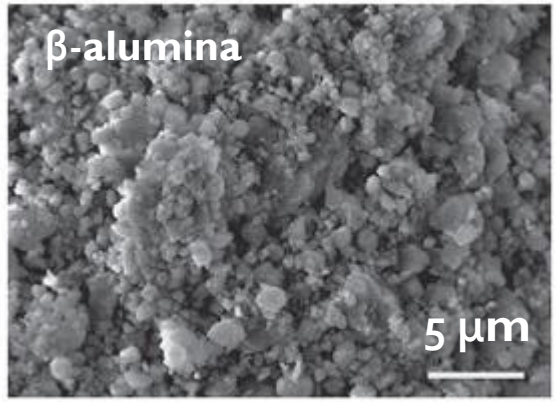

Grain-boundaries among particles clearly observed in the β-alumina pellet

A. Hayashi, Nature Communications 3 (2012) Article number: 856, 1-5.

3

Performances of ASSB

Li-ion, Li-Sulfur and Na-ion batteries

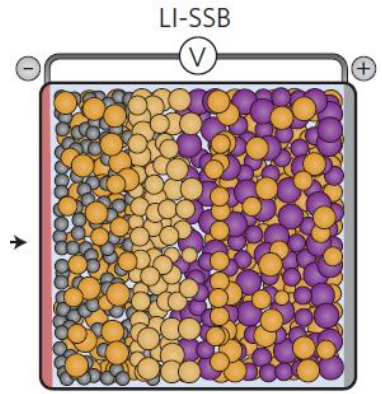

Challenges for the ASSB assembling

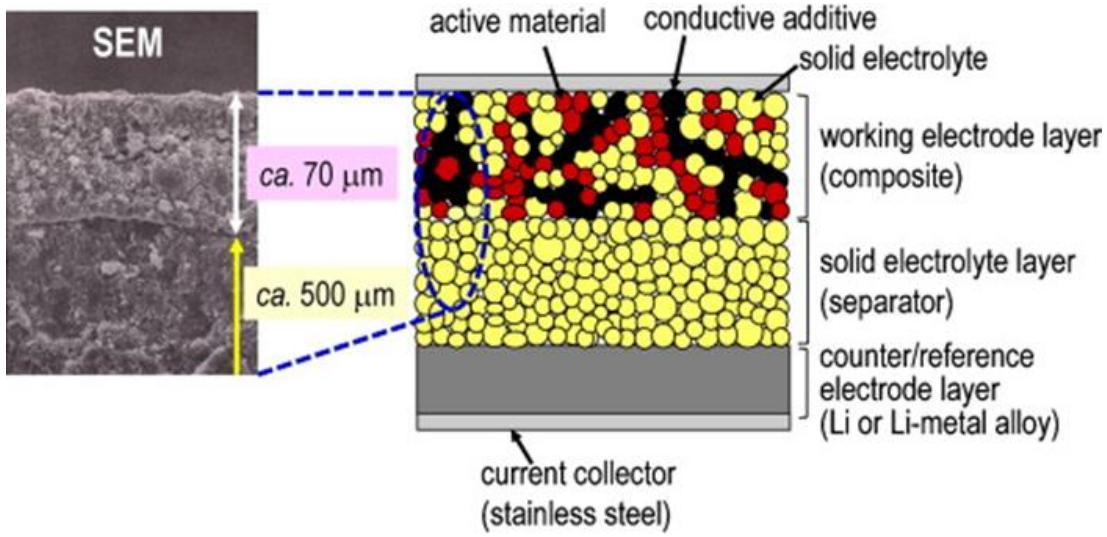

M. Tatsumisago, Journal of Asian Ceramic Societies 1 (2013) 17–25.

Importance of:
- Conductive additives
- Active material
- Binders
- Formulation (ratios of ≠ components)
- Mixting method (hand grinding, turbula,..)

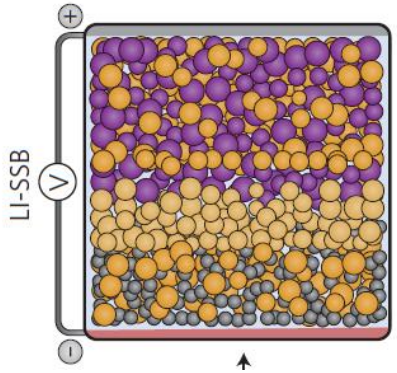

Cathode composite

Solid electrolyte

Anode composite

SEM pictures

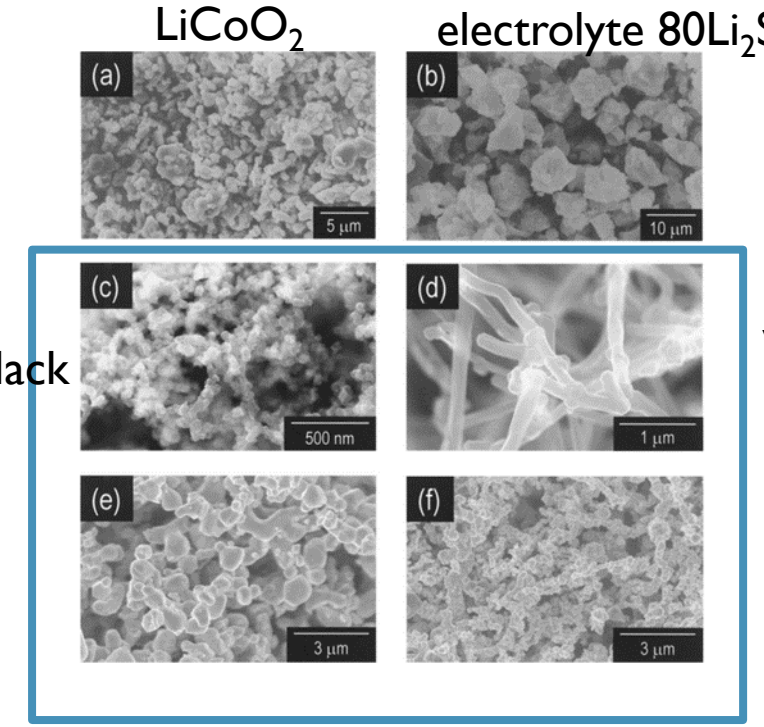

different conductive additives:
acetylene black

VGCF

TiN

Ni

F. Mizuno, Journal of the Electrochemical Society 152(8) (2005) A1499

Li ion batteries: large choice of active materials

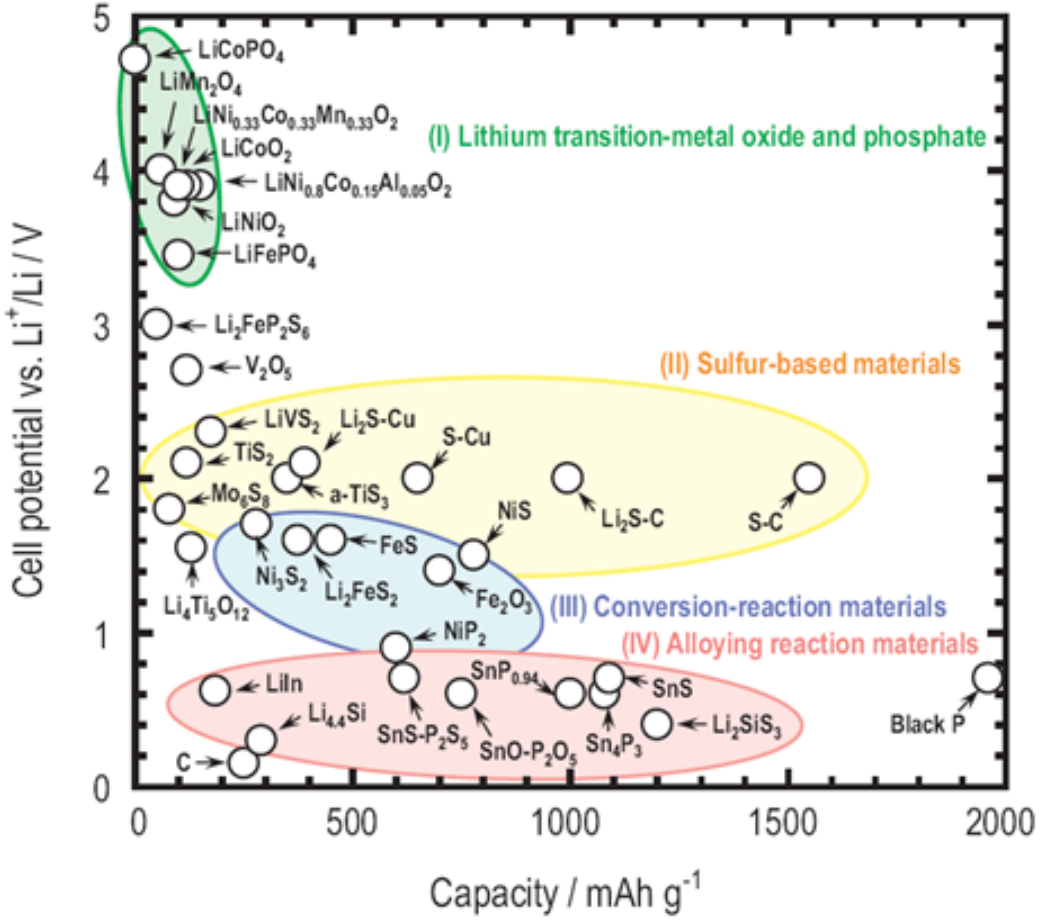

Four categories on the basis of cell potential:

(I) lithium transition-metal oxides and phosphates with a potential of 3.5–5 V (●),
category including high-potential positive electrodes: $LiCoO_2$, $LiNiO_2$, $LiNi_{0.8}Co_{0.15}Al_{0.05}O_2$, $LiNi_{0.33}Co_{0.33}Mn_{0.33}O_2$, $LiMn_2O_4$, $LiFePO_4$ and $LiCoPO_4$.

(II) sulfur-based materials with 2 V (●),

(III) conversion-reaction materials with 1–2 V (●),

(IV) alloying reaction materials with below 1 V (●).

M. Tatsumisago, Journal of Asian Ceramic Societies 1 (2013) 17–25.

Assembling processes

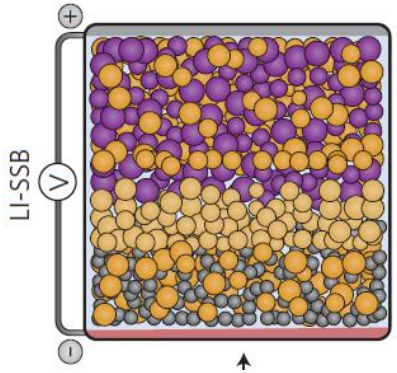

Cathode composite

Solid electrolyte

Anode composite

powder pressing process

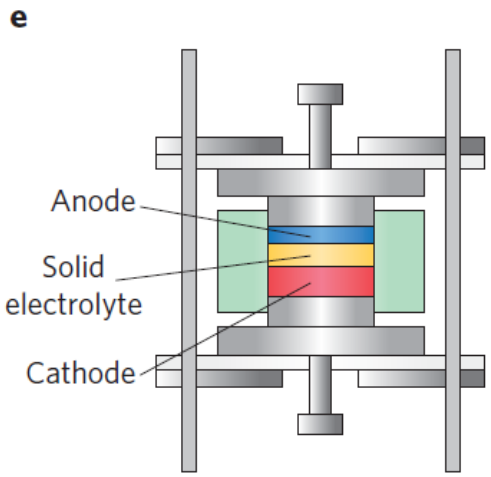

difficult to scale up for practical applications

Some alternative fabrication methods may be considered

pasting route analogous to that used in solid oxide fuel cell fabrication

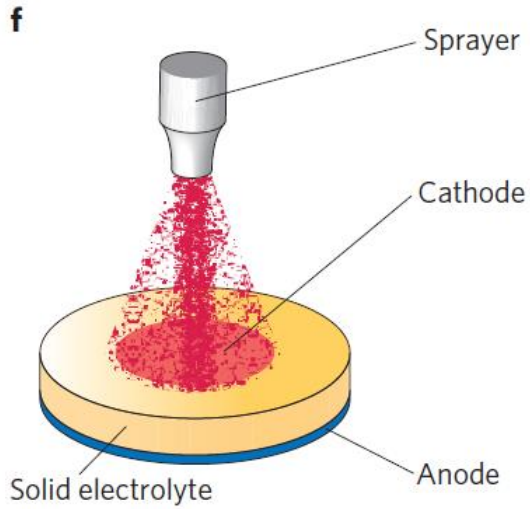

process might be costly.

Solution processed

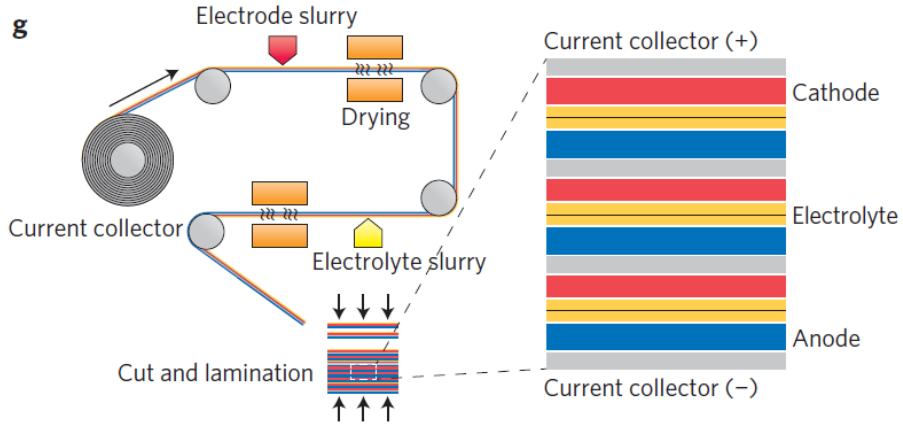

Investigation of solvents of polymer binders

Yong-Sheng Hu, Nature Energy, Vol. 1, 2016, article number: 16042

Charge–discharge curves at the 500th cycle of In/$LiCoO_2$ cells with the $67Li_2S{\cdot}33PS_{2.5}$ (=$80Li_2S{\cdot}20P_2S_5$) glass-ceramic

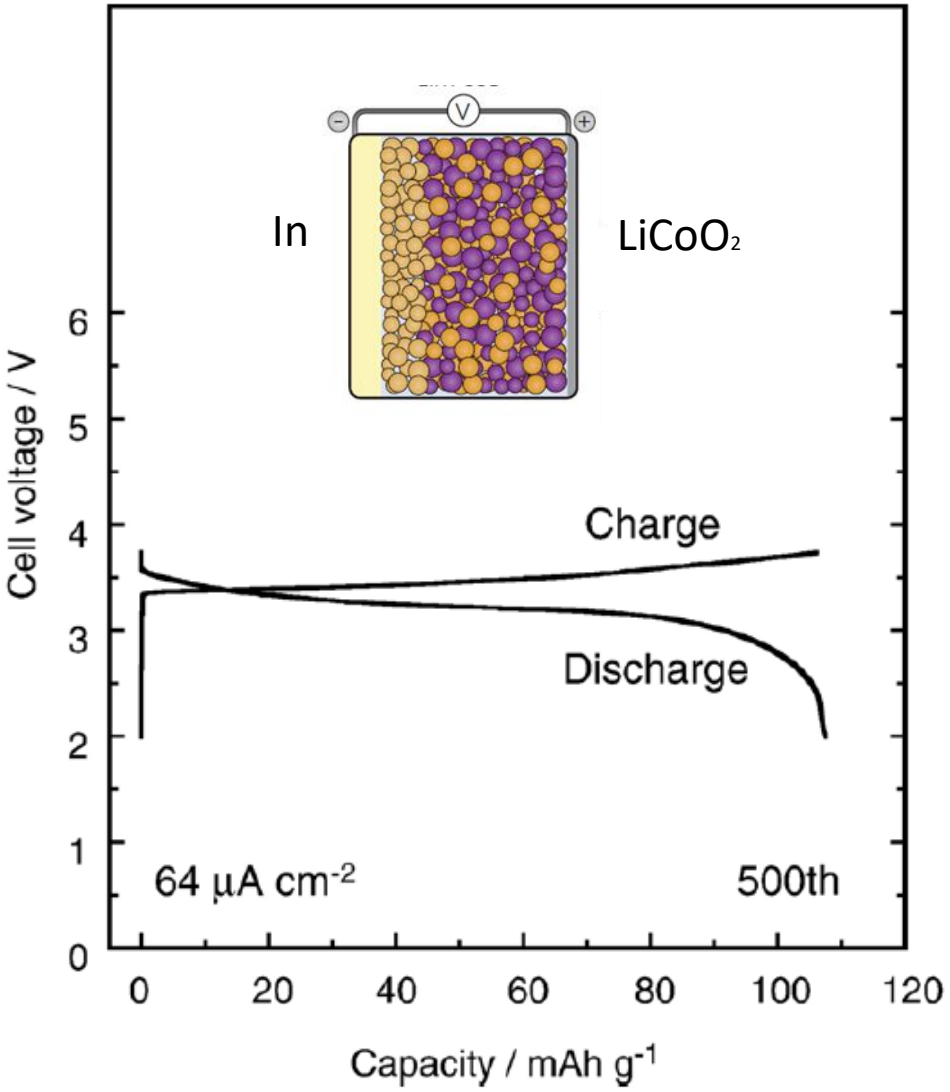

Li-ion batteries

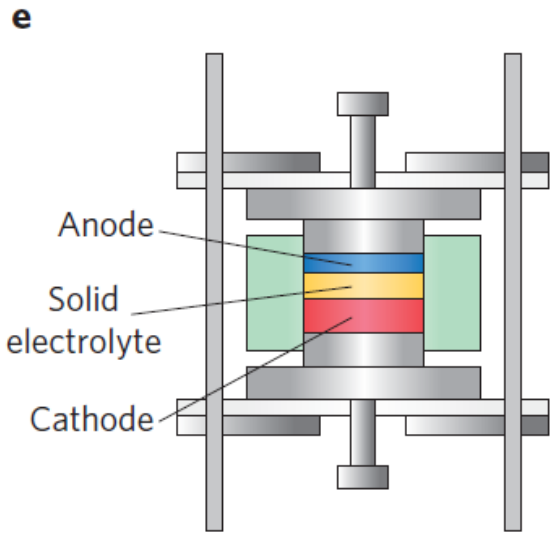

negative electrode
indium foil with a thickness of 0.1 mm pressed under 2.5×10^8 Pa on the pellet

80 mg glass-ceramics powder acting as a solid electrolyte

20 mg composite cathode $LiCoO_2$, glass-ceramics and acetylene-black with the weight ratio of 20:30:3.

⇒ obtained In/$LiCoO_2$ cells charged and discharged at room temperature in an Ar atmosphere (glove-box).

- Irreversible capacity initially observed at the first few cycles,
- The all-solid-state cell maintains the reversible capacity of about 100 mA.h g^{-1}

Recent progress of glass and glass-ceramics as solid electrolytes for lithium secondary batteries. T. Minami et al., Solid State Ionics 2006, 177, 2715–2720.

Charge–discharge curves at the 500th cycle of In/$LiCoO_2$ cells with the $67Li_2S{\cdot}33PS_{2.5}$ (=$80Li_2S{\cdot}20P_2S_5$) glass-ceramic

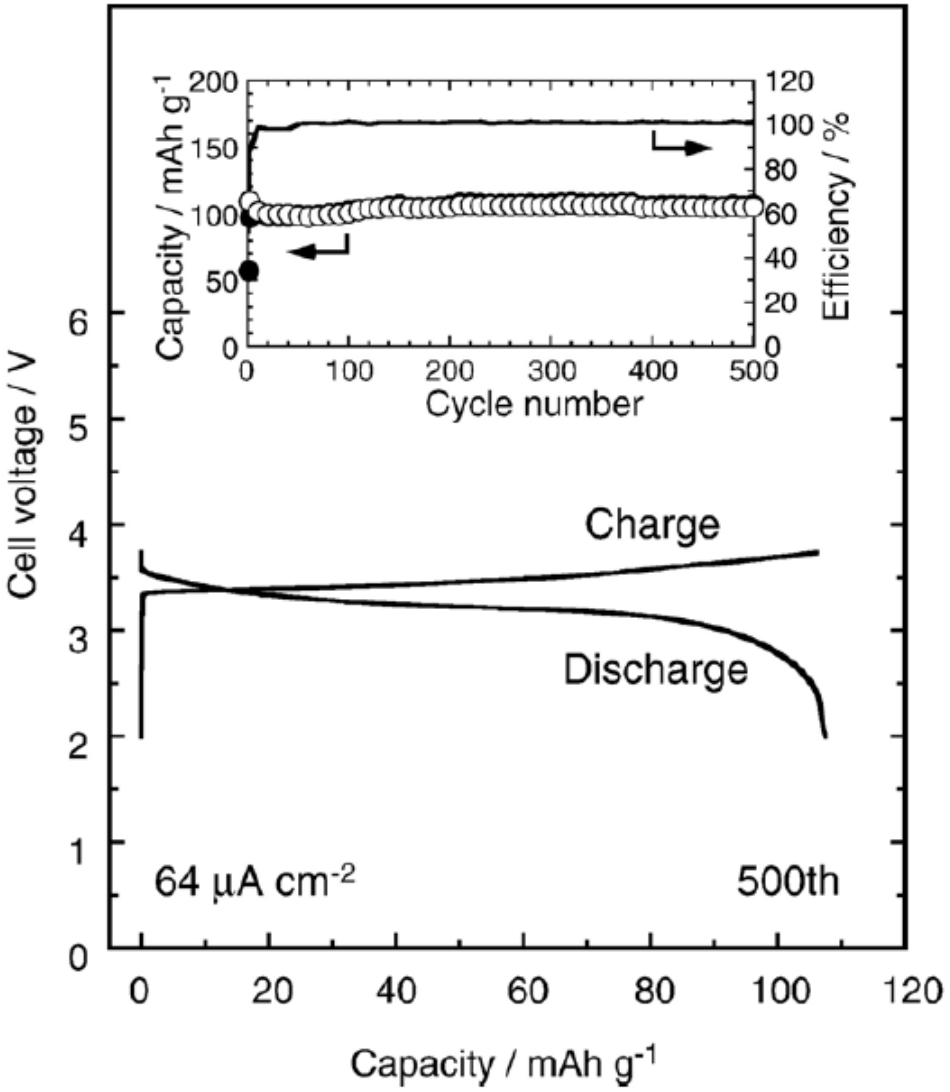

Li-ion batteries

Battery's performance evaluated based on:

Retention of capacity over iterative cycling: Coulombic efficiency (CE)
= percent of specific discharge (A.h/kg or A.h/l) retained upon immediate subsequent charging.
CE is always less than 100% for real SIBs

(Lifetime of a SIB often defined as the number of cycles until the cell only demonstrates 80% of its initial capacity, so a cell which has a lifetime of 500 cycles must have a CE of at least 99.96% for each cycle)

Charge–discharge efficiency of 100% (no irreversible capacity) for 500 cycles,
⇒ the cell works as a lithium secondary battery without the decomposition of the glassy electrolyte.

Recent progress of glass and glass-ceramics as solid electrolytes for lithium secondary batteries.
T. Minami et al., Solid State Ionics 2006, 177, 2715–2720.

Charge–discharge cycle performance of the all-solid-state Li–In/$Li_4Ti_5O_{12}$ cell

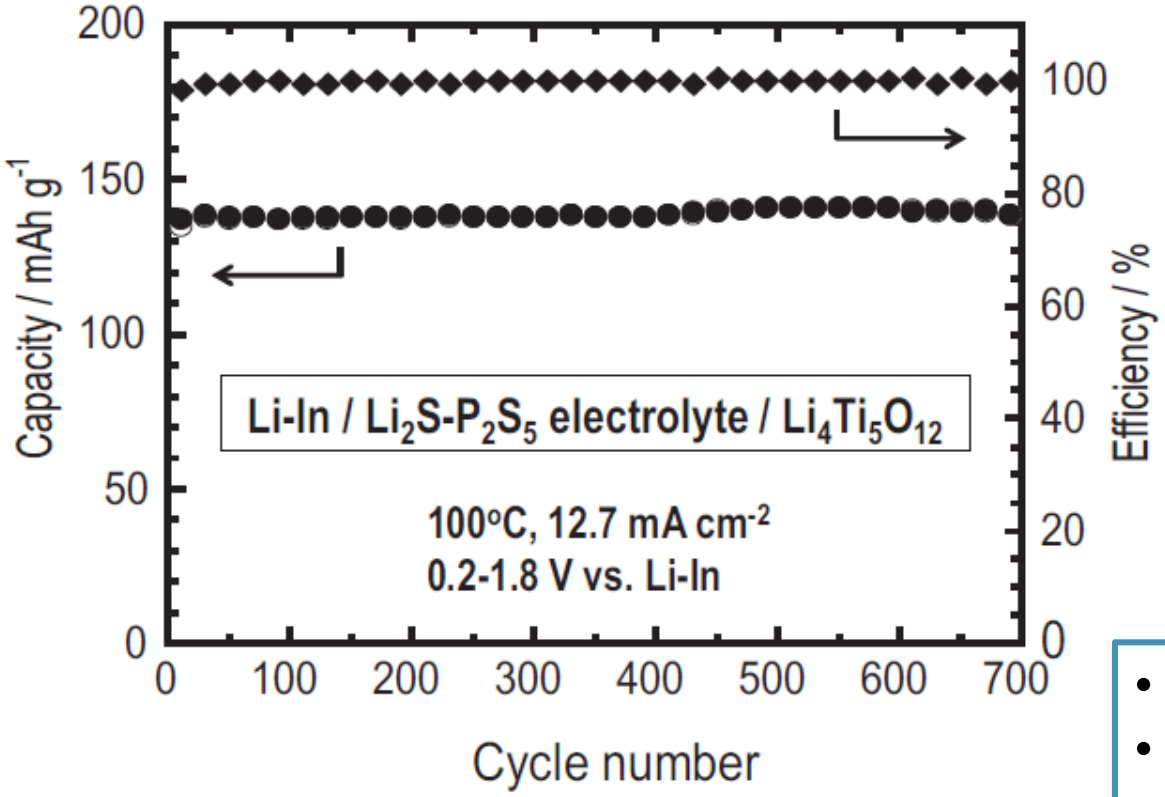

M. Tatsumisago, M. Nagao, A. Hayashi,
Journal of Asian Ceramic Societies 1 (2013) 17–25.

Li-ion batteries

$Li_4Ti_5O_{12}$
Commercialized negative electrode
Moderate potential of 1.55 V (vs. Li^+/Li) but "zero-strain" material during charge–discharge processes

Composite working electrode
= $Li_4Ti_5O_{12}$, Li_2S–P_2S_5 glass–ceramic SE, and vapor grown carbon fiber (VGCF) powders with a weight ratio of 38:58:4

Cycling at 100 ◦C!

- Discharge and charge capacity of about 140 $mAhg^{-1}$
- Capacity maintained for 700 cycles with no degradation under a high current density of over 10 mA cm^{-2}.

⇒ all-solid-state batteries using glass–ceramic electrolytes have a benefit of high temperature application.

Li-sulfur batteries

Initial discharge/charge cycles of Li−In/$Li_7P_3S_{11}$/S−C and Li−In/$Li_7P_{2.9}Sb_{0.1}S_{10.75}O_{0.25}$/S−C batteries at 0.05C rate

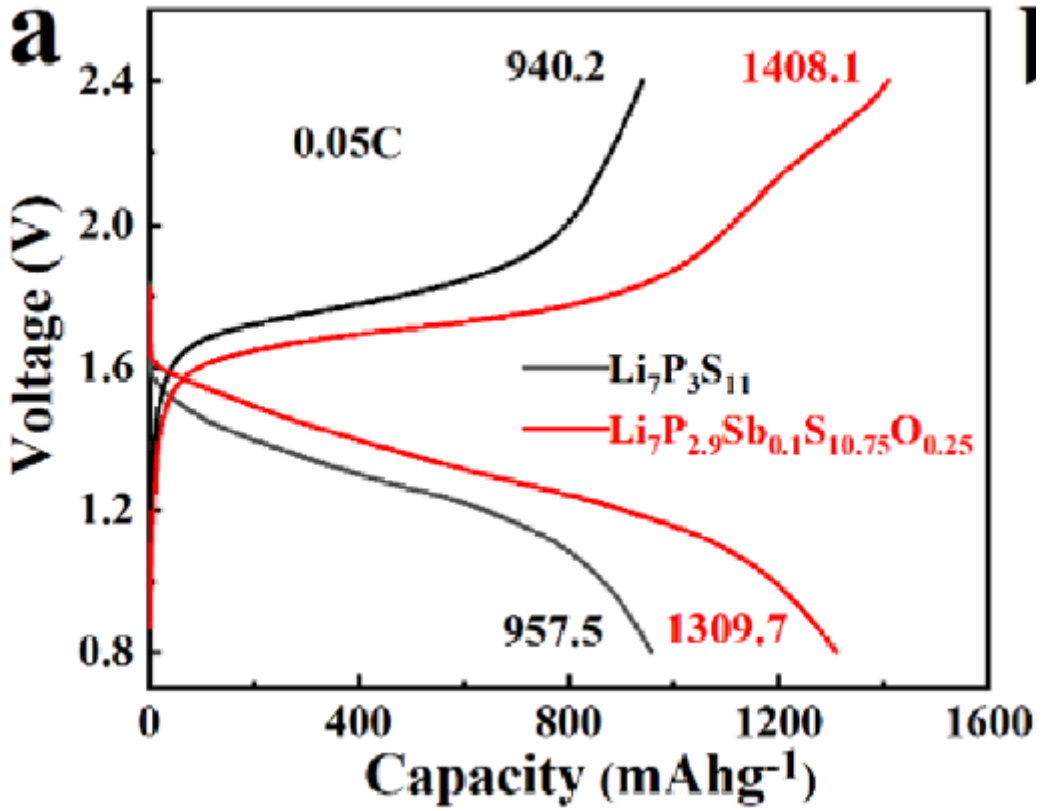

One discharge and charge voltage plateau, corresponding to the reversible electrochemical reaction of S/Li_2S without polysulfide intermediates.

Discharge capacity with the $Li_7P_3S_{11}$ of 957.5 mAh g^{-1}, while that of the one with the $Li_7P_{2.9}Sb_{0.1}S_{10.75}O_{0.25}$ electrolyte can reach 1309.7 mAh g^{-1}

⇒ improved low interface resistance and ionic conductivity.

B.H. Zhao, ACS Appl. Mater. Interfaces 2021, 13, 34477−34485
Congener Substitution Reinforced $Li_7P_{2.9}Sb_{0.1}S_{10.75}O_{0.25}$ Glass-Ceramic Electrolytes for All-Solid-State Lithium−Sulfur Batteries

Li-sulfur batteries

Rate performance of ASSLSBs with $Li_7P_3S_{11}$ and $Li_7P_{2.9}Sb_{0.1}S_{10.75}O_{0.25}$ electrolytes at 0.05C, 0.1C, 0.2C, 0.5C, and 1C rates.

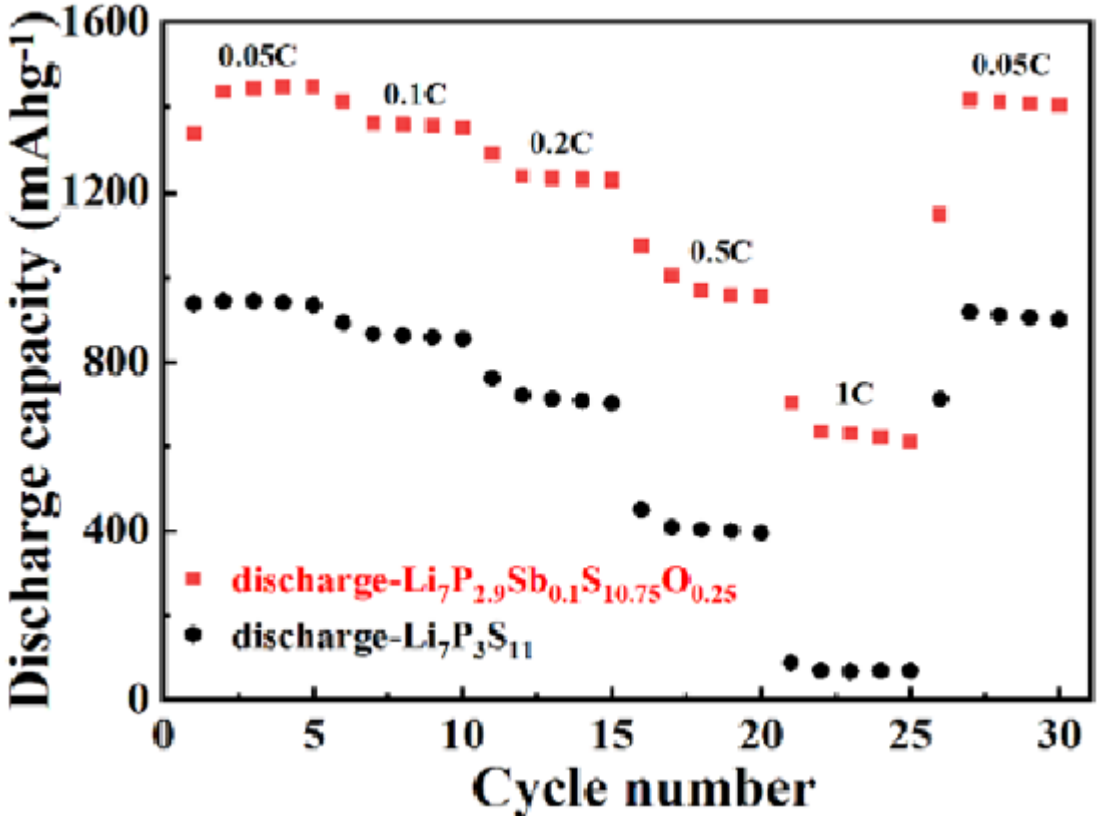

The rate at which SIB can deliver its energy often reported in terms of 'C-rate.'

A c-rate of 1 C refers to the current density (mA/cm^2) delivered by the battery at which the cell would deliver its entire theoretical capacity in a time interval of 1 h.

- Capacities decrease with increasing C-rate but when the rate is switched to 0.05C the capacities could recover to initial values

⇒ good reversibility

- ASSLSBs with $Li_7P_{2.9}Sb_{0.1}S_{10.75}O_{0.25}$ exhibit superior discharge capacities

B.H. Zhao, ACS Appl. Mater. Interfaces 2021, 13, 34477−34485
Congener Substitution Reinforced $Li_7P_{2.9}Sb_{0.1}S_{10.75}O_{0.25}$ Glass-Ceramic Electrolytes for All-Solid-State Lithium−Sulfur Batteries

Li-sulfur batteries

Cycling performance and Coulombic efficiency of ASSLSBs with $Li_7P_3S_{11}$ and $Li_7P_{2.9}Sb_{0.1}S_{10.75}O_{0.25}$ electrolytes at 0.05C rate

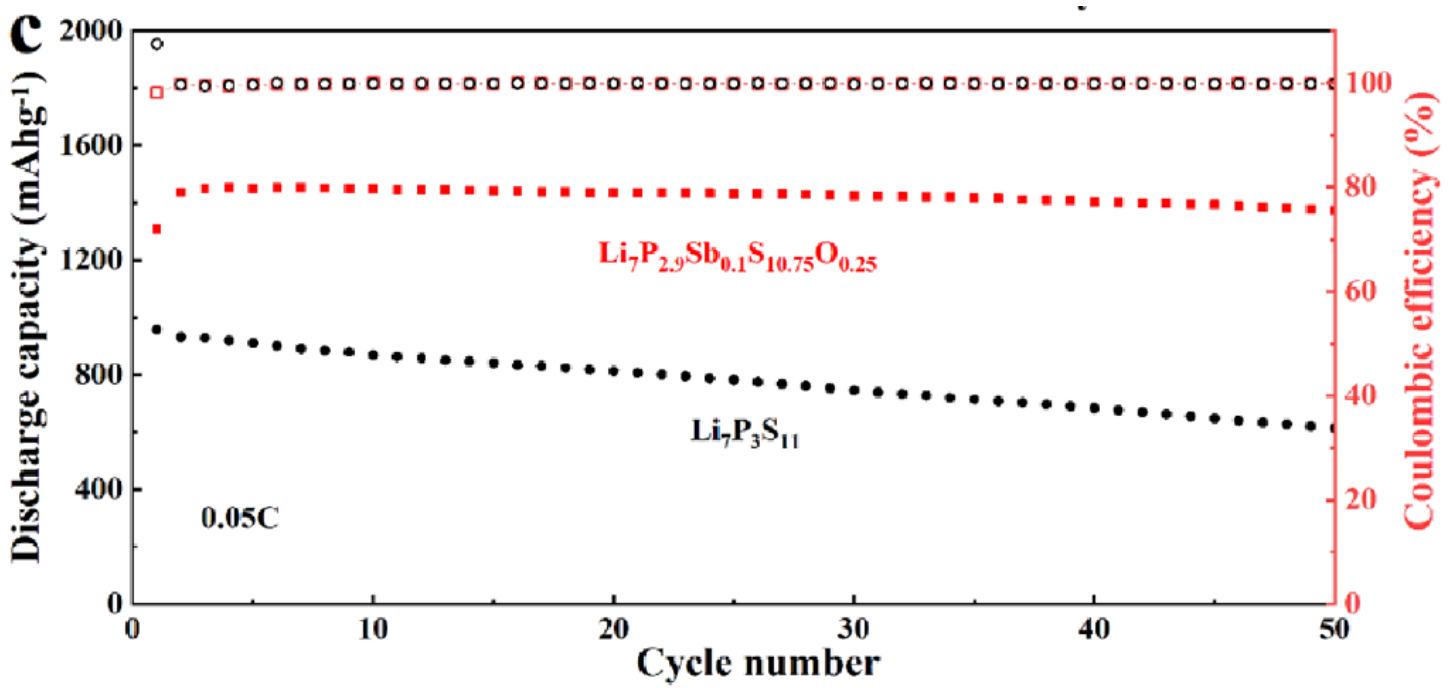

- In the first cycle, large initial charge capacity and low initial Coulombic efficiency

⇒ Unstable solid−solid interface between the cathode/anode and sulfide electrolyte

- After the activation process, the battery can be charged/discharged normally with high Coulombic efficiency.

- Fast capacity decline for $Li_7P_3S_{11}$ contrary to $Li_7P_{2.9}Sb_{0.1}S_{10.75}O_{0.25}$

B.H. Zhao, ACS Appl. Mater. Interfaces 2021, 13, 34477−34485
Congener Substitution Reinforced $Li_7P_{2.9}Sb_{0.1}S_{10.75}O_{0.25}$ Glass-Ceramic Electrolytes for All-Solid-State Lithium−Sulfur Batteries

Na batteries

The relationship between capacity and voltage for present electrode materials in Na-ion batteries

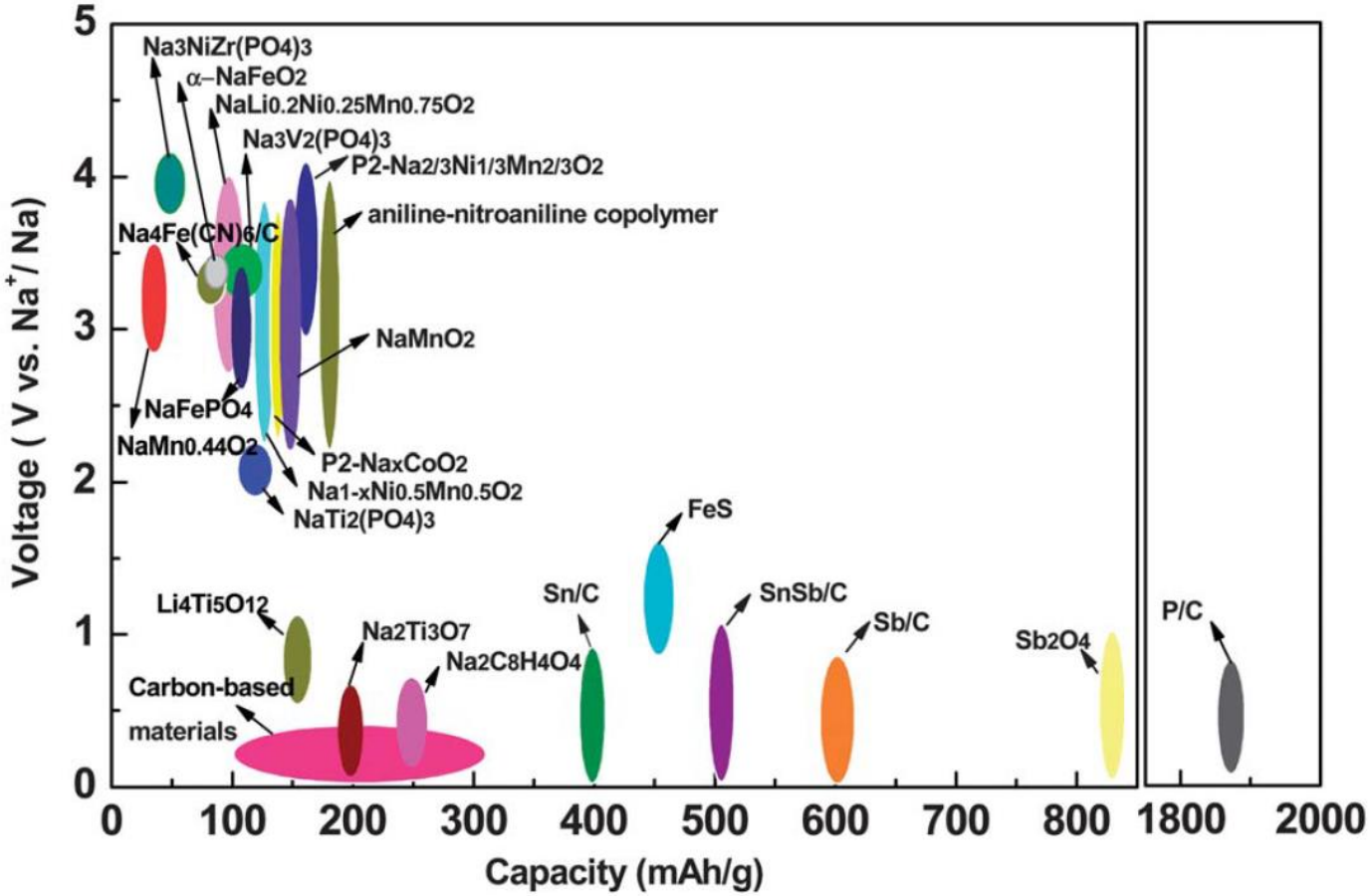

Room-Temperature Stationary Sodium-Ion Batteries for Large-Scale Electric Energy Storage
H. Pan, Energy Environ. Sci., 2013, 6, 2338

Na batteries

Cathode composite

Chevrel phase Mo_6S_8 ~1.4 V (vs Na/Na^+)
coated with a thin layer of Na_3PS_4
+ Na_3PS_4 glass-ceramic
+ Acetylene black

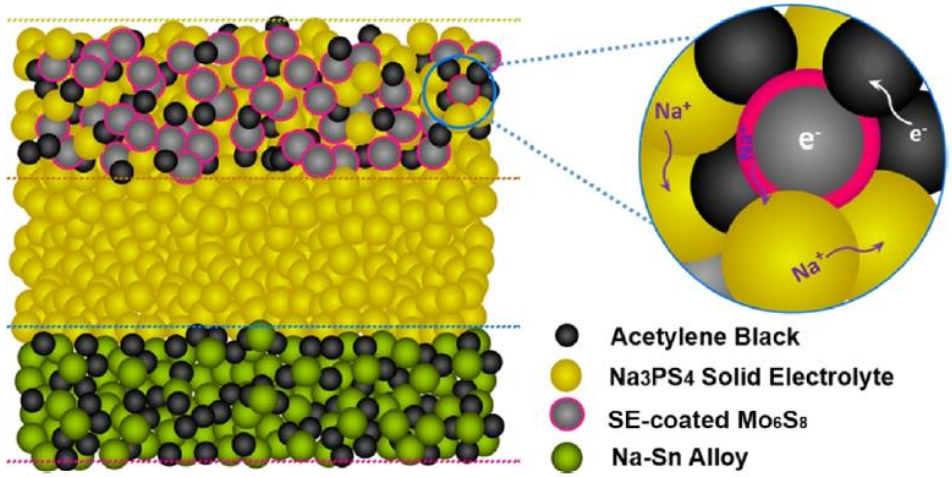

Anode composite

Na-Sn alloy
Acetylene black

Charge–discharge profiles
at various current densities from 5 to 60 $mA.g^{-1}$

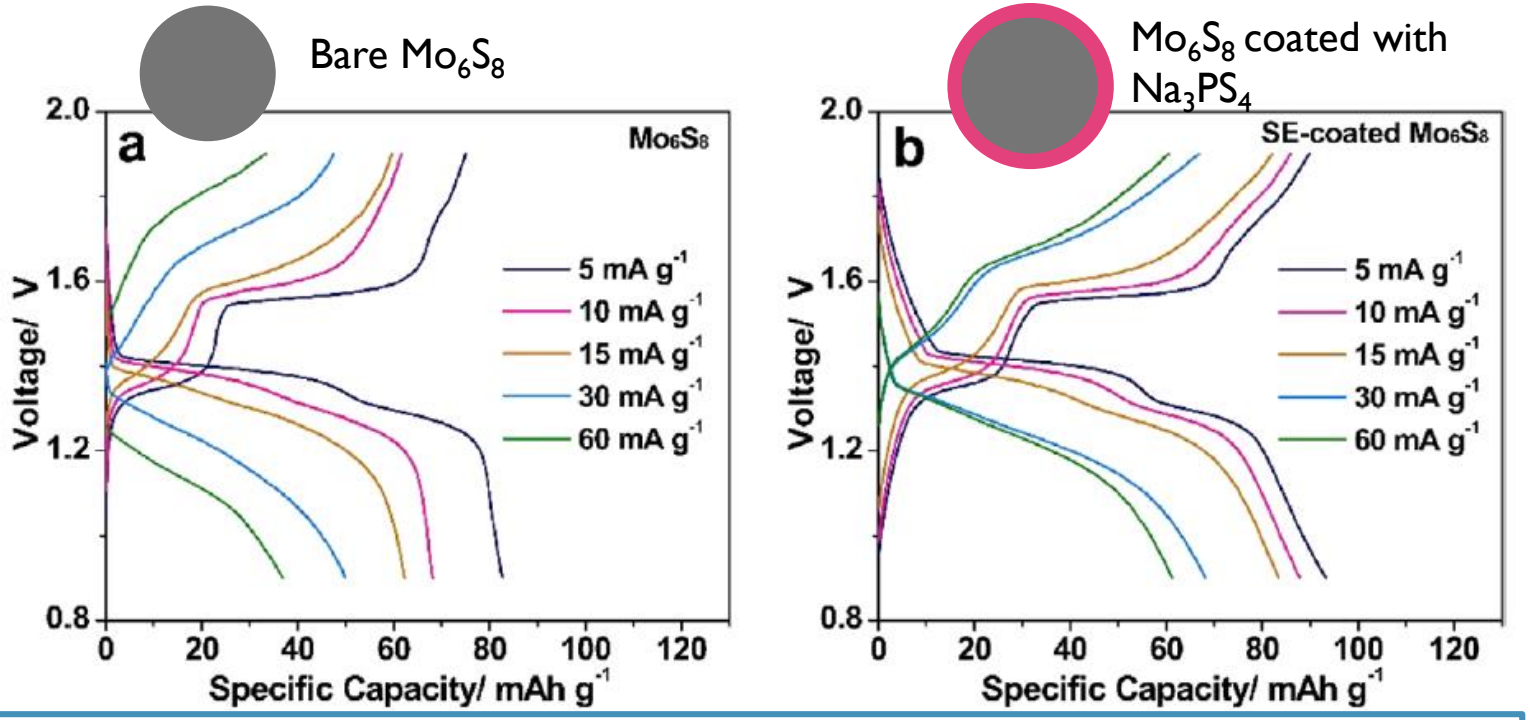

- Decrease of the capacities with increasing currents
- The SE-coated Mo_6S_8 electrode delivers higher capacities than the bare Mo_6S_8 electrode at the same currents.

⇒ Enhanced rate performance of SE-coated Mo_6S_8

Long Cycle Life All-Solid-State Sodium Ion Battery
J.Yue, ACS Appl. Mater. Interfaces 2018, 10, 39645−39650

Na batteries

Cycling performances and Coulombic efficiencies of the Mo_6S_8 and SE-coated Mo_6S_8 cathodes in ASIBs at 60 mA.g^{-1} at 60 °C.

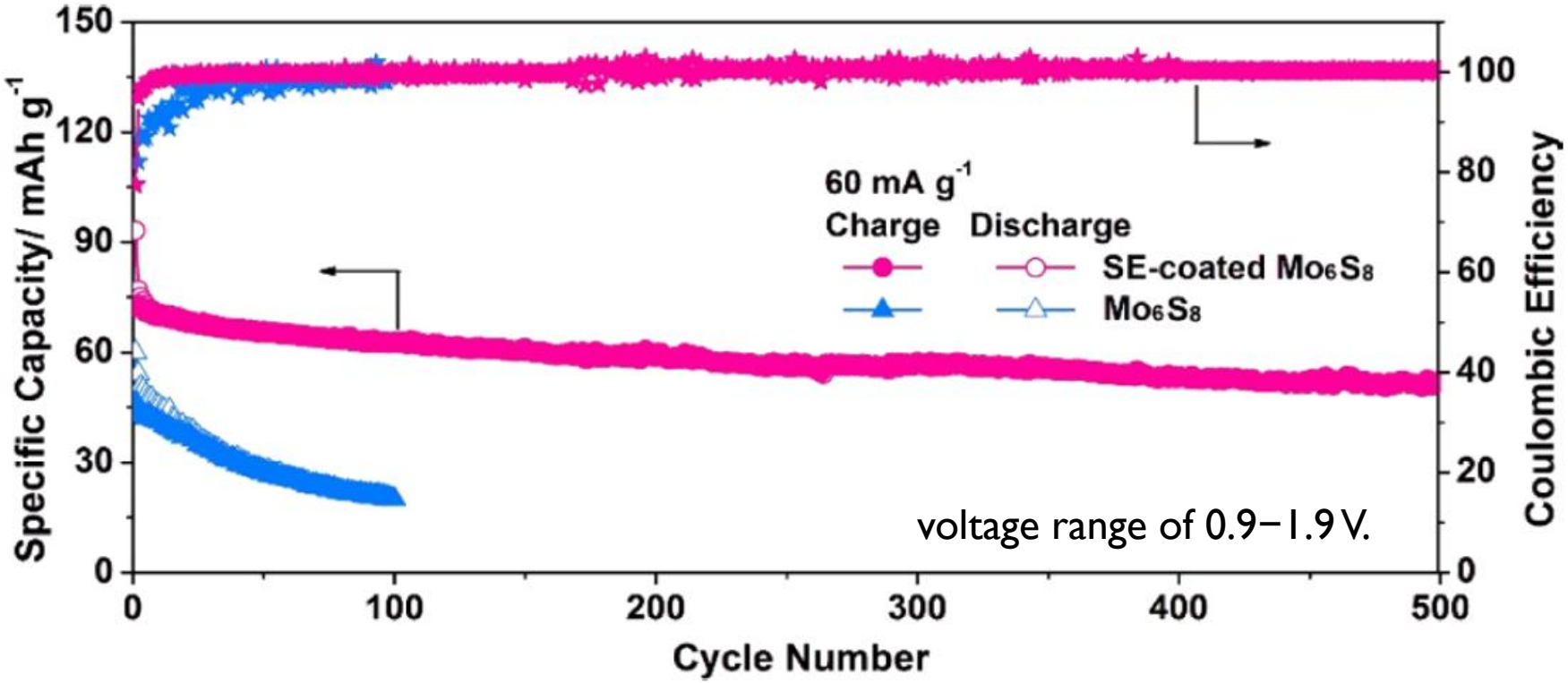

- Limited potential (voltage range of 0.9−1.9 V) but high cycling performance (500 cycles)
- Thin layer of Na_3PS_4 coated on Mo_6S_8 ⇒ solution method to achieve an intimate contact between Mo_6S_8 and the SE

Long Cycle Life All-Solid-State Sodium Ion Battery
J.Yue, ACS Appl. Mater. Interfaces 2018, 10, 39645−39650

4

Conclusions and perspectives

Glass and glass-ceramic solid electrolytes

New synthetic routes
Since the 2000s

Ball-milling

thermal-image furnace
and twin roller

Melting
+ quenching

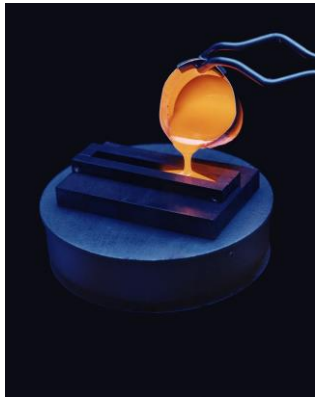

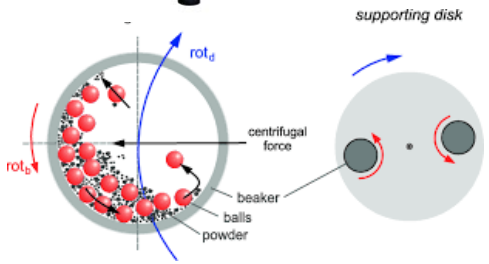

Solvent assisted synthesis

- Glass-ceramics
  - 80-20 Li_2S-P_2S_5
  - 70-30 Li_2S-P_2S_5
  - $Li_7P_3S_{11}$
  - Argyrodite
- Superionic conductive crystal
  - $Li_7P_3S_{11}$
  - Na_3PS_4
- Stable crystalline phase with lower Grain-Boundary resistance
  - LATP
  - LAGP

- Air stability and Li metal compatibility in sulfide based solid electrolytes
  - P substitution by Sn, Sb and Zn
  - S substitution by O

Challenges for the ASSB assembling

Large choice of active materials

Different technologies

- **Na**
- **Li**
- **Li-S**

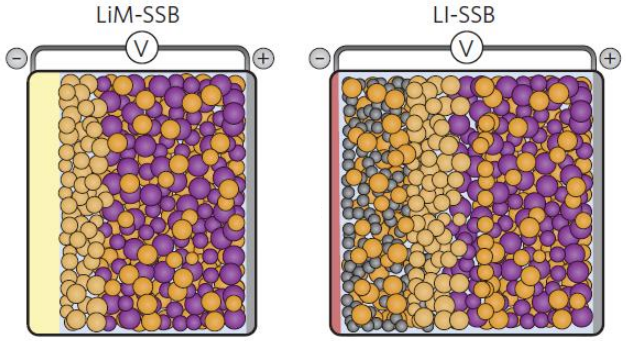

Cycling possible at high temperature

Strategies to improve interface (coating)

Assembling processes

powder pressing process

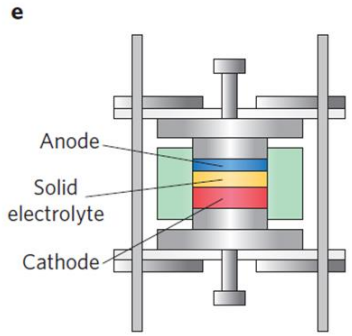

Scalability

Solution processed

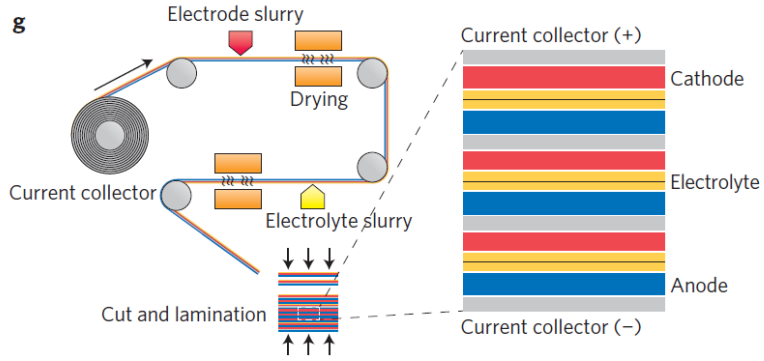

Solid electrolytes suppliers

Ampcera™

https://ampcera.com/

MSE Supplies
We Enable Innovations

Call Us: +1 (520)789-6673 Sign in or Create an Account

Search all products... Cart

HOME PRODUCTS CUSTOMIZATION ABOUT CONTACT REQUEST A QUOTE WHY US OFFERS

Home > Solid Electrolyte Materials

Shop By

- Al-doped LLZO
- Argyrodite
- Ga-doped LLZO
- GeS2 Powder
- LAGP
- LATP
- LGPS
- Li2S Powder
- Li6PS5Br
- Li6PS5Cl
- Li6PS5Cl0.5Br0.5
- LISICON membrane
- Lithium Phosphate (Li3PO4) LiPON
- LLZO
- LPS
- LSPS
- NASICON Na3Zr2Si2PO12
- Nb-doped LLZO
- Oxide Ceramic Sputtering Targets
- PEO
- Sodium Beta Alumina
- Sodium Ion Battery

Solid Electrolyte Materials

Ampcera™ solid state electrolyte materials are used in all-solid-state Lithium batteries and other advanced lithium batteries. Compared to a liquid electrolytes, battery a solid electrolyte battery has the advantages of higher energy density (~2X), better safety, and long term stability. Commonly studied solid electrolyte materials include sulfide compounds (e.g. Argyrodite, LGPS, LPS, etc.), garnet structure oxides (e.g. LLZO with various dopants), NASICON-type phosphate glass ceramics (LAGP), oxynitrides (e.g. lithium phosphorus oxynitride or LIPON), and polymers (PEO). The lithium ionic conductivity of the inorganic solid electrolyte materials ranges from 10^{-4} S/cm up to 10^{-2} S/cm at room temperature. MSE Supplies also offers sodium beta alumina solid electrolyte powder.

Because of the high ionic conductivity and stable quality, Ampcera™ solid state electrolyte materials have been used by many well-known companies and research labs worldwide for the development and manufacturing of advanced lithium batteries. Both standard and customized solid state electrolyte materials are offered to meet customer's specific requirements for R&D and production. Products can be ordered as little as a few grams or as much as 100 kg with consistent quality.

Order your solid state battery materials today or discuss with our materials scientists about your specific project needs.

Sort by Alphabetically, A-Z

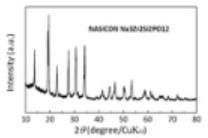

50g NASICON

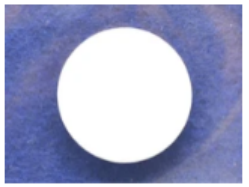

Ampcera LISICON LATP

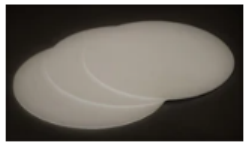

Ampcera™ Al-LLZO

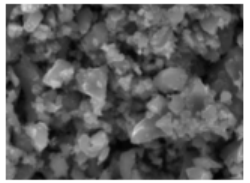

Ampcera™ Argyrodite

Developers of solid-state batteries

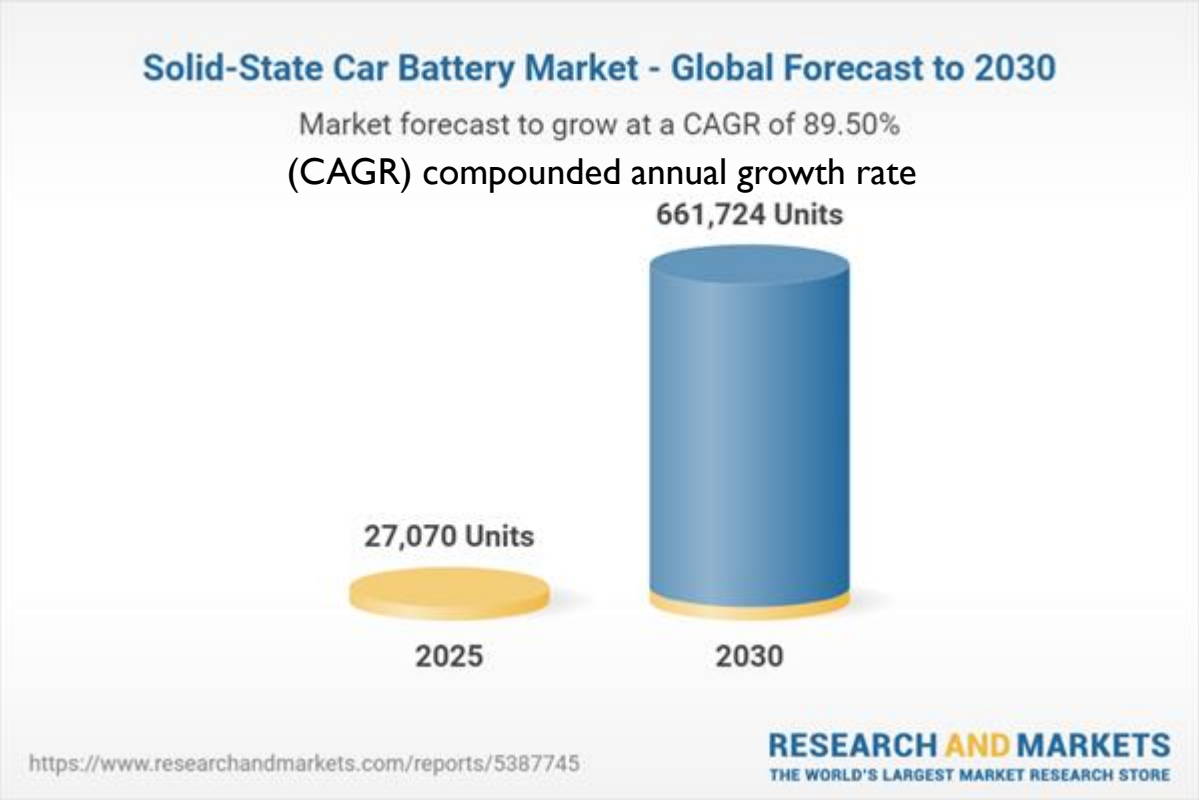

Company Profiles Key Players

- Toyota Motor Corporation
- Solid Power
- Quantumscape
- Samsung Sdi
- LG Chem
- Ilika
- Brightvolt
- Panasonic
- Catl
- Ioniq Materials
- Northvolt
- Cymbet

https://solidpowerbattery.com/

Bibliography

In addition to the references already given at the bottom of the slide

Emerging Role of Non-crystalline Electrolytes in Solid-State Battery Research
Zane A. Grady *et al*,. Frontiers in Energy Research, Volume 8, Article 218, 2020

Towards Higher Electric Conductivity and Wider Phase Stability Range via Nanostructured Glass-Ceramics Processing
Tomasz K. Pietrzak *et al*., Nanomaterials 2021, 11, 1321

Inorganic sodium solid-state electrolyte and interface with sodium metal for room-temperature metal solid-state batteries
Jin An Sam Oh *et al*., Energy Storage Materials 34 (2021) 28–44

Interfaces and Interphases in All-Solid-State Batteries with Inorganic Solid Electrolytes
Abhik Banerjee et al.,

APPLICATION: MATERIALS FOR ENERGY ELECTROLYTES FOR ALL-SOLID-STATE BATTERIES

VIRGINIE VIALLET

Thanks for your attention